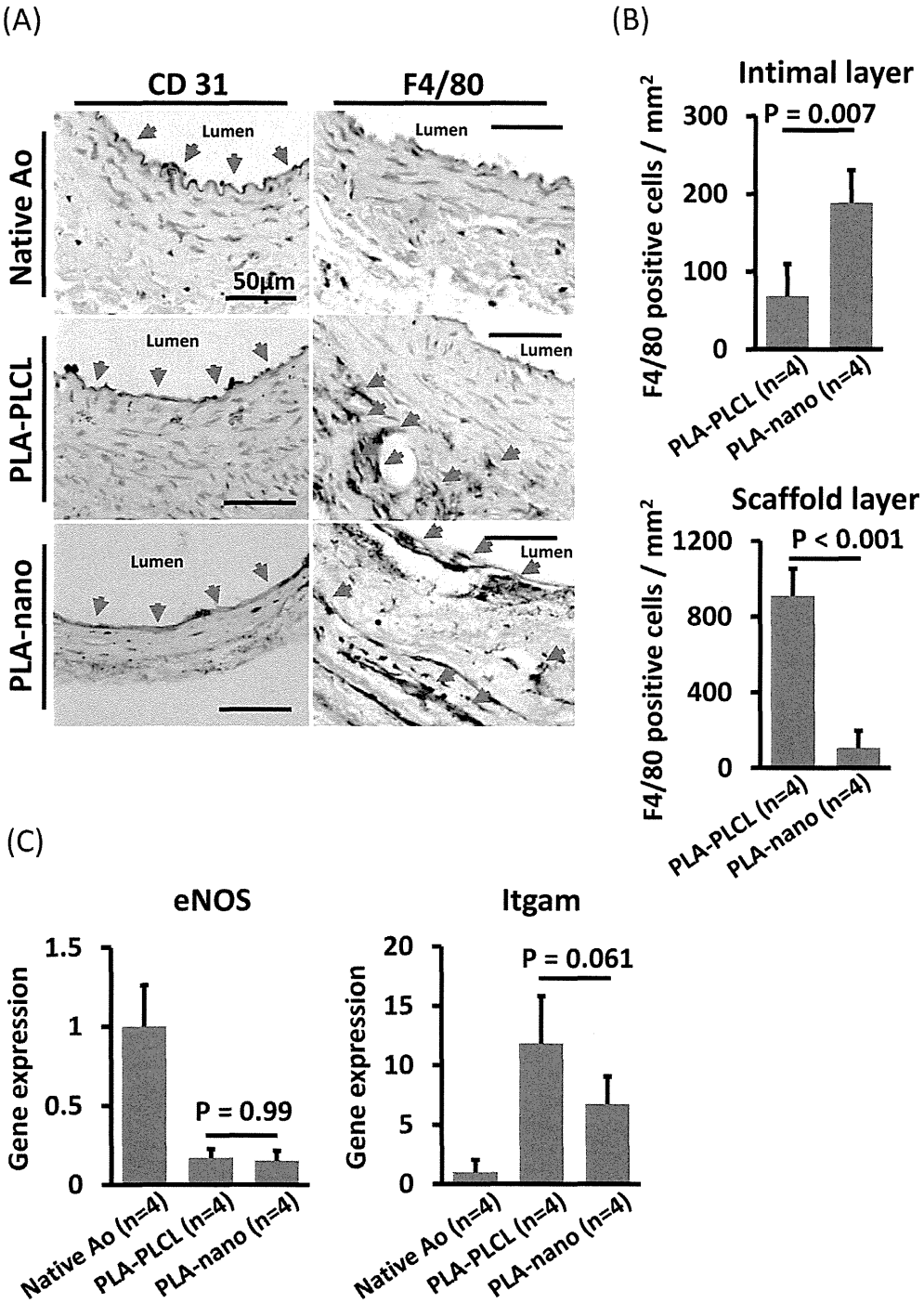

Fig. 4. Endothelialization and macrophage infiltration of the grafts at 12 months after implantation. (A) Representative histological image of (left) endothelial cell staining (CD 31) and (right) macrophage staining (F4/80). CD31 staining showed endothelial cell coverage of luminal surface in both groups, and F4/80 staining demonstrated a difference in macrophage localization between both groups. (B) The number of F4/80 positive cells (/mm^2) was counted for the quantitative analysis of macrophage infiltration into scaffold using immunohistochemical staining images (mean ± standard deviation), and evaluated by student's *t* test. In the intimal layer, the density of macrophages in PLA-nano grafts was higher than that of PLA–PLCL grafts, although, in the scaffold layer, more macrophages existed around the remaining PLA fibers in PLA–PLCL grafts compared to PLA-nano grafts. (C) Gene expression was analyzed by RT-qPCR using the ΔΔ CT method. Data are expressed as fold change over native aorta expression (mean ± standard deviation), and evaluated by one-way ANOVA followed by Tukey HSD. There was no significant difference of gene expression of eNOS or Itgam between two groups.

3.7. Expression of transcription factors for osteogenesis and osteoclastgenesis in vascular smooth muscle cells

Osteogenic progenitors are thought to arise from trans-differentiation of mature VSMCs, and Runx2 and BMP2 are transcription factors of this lineage [10]. RANKL is one of the key transcription factors associated with osteoclast differentiation [11].

Runx2 and RANKL were increased in the neointima of PLA–PLCL (Fig. 6A), and smooth muscle cells, defined by SMA positive cells, expressed both of these factors 12 months after implantation (Fig. 6B). Furthermore, RT-qPCR revealed that gene expression of Runx2 and RANKL in PLA–PLCL were higher than those in PLA-nano(Runx2, PLA–PLCL: 15.8 ± 3.33 vs PLA-nano: 1.44 ± 0.71, $P < 0.001$; RANKL, PLA–PLCL: 10.9 ± 1.86 vs PLA-nano: 0.60 ± 0.43,

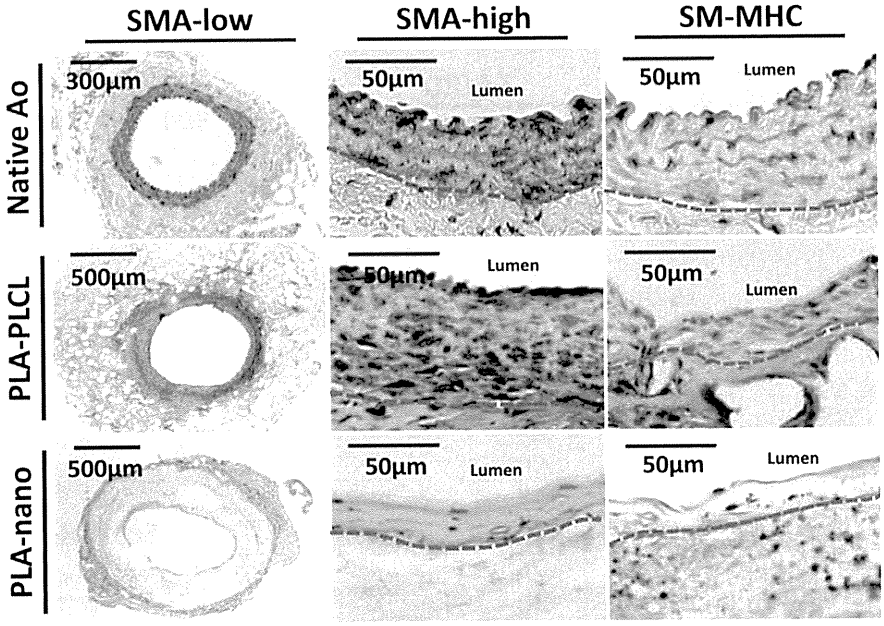

Fig. 5. Vascular smooth muscle cell proliferation in neointima of PLA–PLCL graft at 12 months after implantation. Immunohistochemical staining with low and high power magnifications of smooth muscle actin (SMA) and of smooth muscle myosin heavy chain (SM-MHC) demonstrated abundant VSMCs in neointima of PLA–PLCL grafts, although, few cells positive for these markers were found in the thin neointimal layer of the PLA-nano grafts.

$P < 0.001$) (Fig. 6C), although, no difference was observed between groups in gene expression of BMP2 12 months after implantation (PLA–PLCL: 1.13 ± 0.24 vs PLA-nano: 0.82 ± 0.23, $P = 0.11$) (Fig. 6C).

4. Discussion

Calcific degeneration remains one of the major obstacles facing the translation of TEVGs for arterial repair [12]. In this study, we demonstrated little evidence of calcification in the neointimal layer of large-pore PLA–PLCL grafts. In contrast, severe calcification occurred in the thin neointimal layer of the small-pore electrospun PLA-nano graft. Poly(L-lactic acid) (PLA) and poly(caprolactone) (PCL) are commonly used biodegradable materials for constructing arterial scaffolds due to their history of successful clinical usage [13]. Combining these materials with additional synthetic polymers to create copolymers such as poly(L-lactic-co-ε-caprolactone) (PLCL) allows for rational tuning of mechanical properties and degradation rates through precise control of polymer composition ratios and molecular weights. We created the seamless PLA–PLCL conduit by sealing PLA mesh with a PLCL solution. Since the relative mass of PLCL sealant was much lower than that of the PLA mesh in the PLA-PCLA graft (Fig. 1), we argue that the PLA is the dominating polymer in this scaffold. Furthermore, our previous studies have shown that the PLCL coating completely degrades 4 months after implantation in a mouse model identical to that presented in this study [9].

In the present study, neotissue formation in the PLA-nano group was inhibited, we observed abundant remaining scaffold fibers, and inflammation in the thin neointima of the PLA-nano group was sustained 12 months following implantation. Nano-fibers created by an electrospinning technique are thought to be a desirable material for fabricating arterial conduits, because they yield scaffolds of high porosity, large surface area, and very small fiber sizes, which are characteristics comparable to fibrils of extracellular matrix components in human tissues [14]. Additionally, they have been shown to improve endothelialization [15] and achieve clinically sufficient burst pressures [16]. Nano-fiber based scaffolds using biodegradable polymers have become a commonly proposed technique for constructing tissue engineered arterial grafts, and have demonstrated favorable surgical and mechanical properties with a high patency rate in arterial implantation models [17–19]. Primary characteristics of graft remodeling, such as luminal endothelialization, transmural cellular ingrowth, and neocapillary formation within the scaffold, dynamically progress according to the degradation rate of the scaffold [20]. Wu et al. demonstrated that a novel, fast degrading elastomer developed well-organized neotissue in a rapid remodeling process without any calcification in a rat aortic implantation model [21]. In contrast, the high density (small pore size) of the nanofiber fabric used in the current study appears to have a long period of polymer degradation without transmural cellular migration into the scaffold. We suggest that the combined effect of slow degradation and low porosity elicited a prolonged foreign body reaction and neotissue remodeling resulting in calcified depositions. A review of existing literature supports our findings, as many groups using electrospun TEVGs with fiber diameters of less than 1 μm demonstrated little or no cellular infiltration [22]. Our previous work indicates that cellular infiltration is critical in generating viable vascular neotissue [23]. Furthermore, macrophage related inflammation is understood to be a key contributor to osteogenesis in early stages of atherosclerotic intimal calcification [24], although, we did not collect data analyzing macrophage phenotype as it relates to calcification in the present study.

The thin intima of PLA-nano grafts had components of extracellular matrix including collagen and elastin, but few VSMCs were observed when compared to that of PLA–PLCL grafts. While VSMC proliferation can lead to neointimal hyperplasia, our results indicate that there was a negative correlation between intimal thickness and calcification area in the graft. Since normal VSMCs have a potential to prevent calcium deposition, some degree of neointimal VSMC proliferation may be required to prevent calcification.

On the other hand, several studies have demonstrated that VSMCs can undergo osteogenic differentiation and calcification [25,26], although the precise mechanisms underlying osteogenic

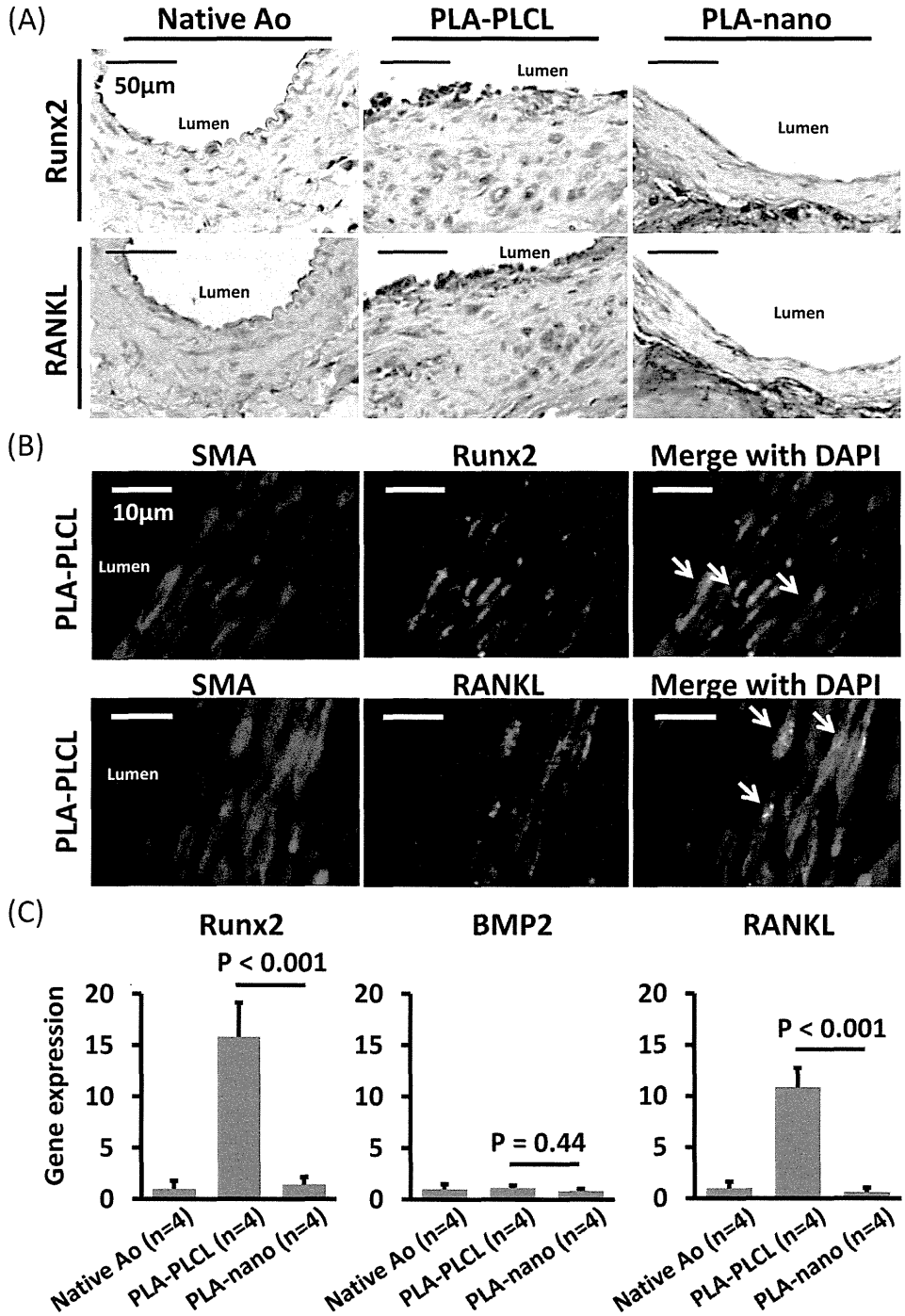

Fig. 6. Expression of transcription factors of osteoblasts (Runx2) and osteoclasts (RANKL) in smooth muscle cells within neointima at the 12 month time point. (A) Immunohistochemial staining revealed that both Runx2 and RANKL were increased in the neointima of PLA–PLCL grafts. (B) Smooth muscle cells, defined by SMA positive cells, expressed both of these factors. (C) Gene expression was analyzed by RT-qPCR using the ΔΔ CT method. Data are expressed as fold change over native aorta expression (mean ± standard deviation), and evaluated by one-way ANOVA followed by Tukey HSD. Runx2 and RANKL in PLA–PLCL grafts were higher than those in PLA-nano grafts, although, no significant difference was found in expression of BMP2.

differentiation of vascular cells during atherosclerosis remain undefined. In the present study, neointimal VSMCs of PLA–PLCL expressed both Runx2 and RANKL, consistent with contractile markers specific to smooth muscle. During the process of vascular calcification, VSMCs can lose their lineage markers such as SMA and SM-MHC, and gain osteogenic makers. Runx2 is thought to be an early marker of VSMC transdifferentiation, is implicated in osteogenic differentiation and calcification of VSMCs, and the upregulation of Runx2 is associated with arterial calcification [25,27]. RANKL is a member of the tumor necrosis factor superfamily, which is the key regulator for osteoclast formation. Under atherosclerotic conditions, mineral resorption by osteoclasts is delicately balanced to maintain osteogenesis with mineral deposition by osteoblasts [28]. One study demonstrated that expression of RANKL in VSMCs was enhanced by Runx2 via a direct binding to the RANKL promoter [29]. One possible reason that such little

calcific deposition was observed in the neointima of our PLA–PLCL grafts even after 12 months is that the upregulation of both osteogenesis and osteoclastgenesis eliminated calcium deposition.

Although well-organized neointima was demonstrated in large pore PLA–PLCL graft, aneurysmal rupture was observed in 46% of implanted those grafts. To solve this issue, TEVG design may require two approaches, including stronger reinforcement, such as combinational use of electrospinning, and improvement of cellular growth and extracellular matrix deposition into the scaffold [9]. We utilized SCID/Bg mice according to our previous experience demonstrating lower rates of TEVG thrombosis and stenosis when implanted in this strain, and this specific model might have affected the results of the current study. Based on this limitation, we have since developed an aortic implantation model for TEVG in the wild type C57BL/6 mouse by using anti-platelet and anti-coagulant drugs to reduce acute thrombosis and stenosis following TEVG implantation. PLCL or its degradation products might affect cell migration, proliferation, or differentiation in the remodeling neotissue, and could lead to development of long-term calcific deposition. Finally, we recognize that the results of the present study do not clearly support an optimal scaffold material or material structure for creation of arterial TEVG; we have identified two ends of a design spectrum within which the ideal arterial TEVG scaffold is situated. Further research is now required to isolate parameters in addition to porosity, such as degradation kinetics, polymer type, and mechanical profile, which in combination will yield an optimized arterial scaffold.

In conclusion, the present study demonstrated that large-pore PLA grafts with a PLCL coating (PLA–PLCL) created a well-organized neointima and prevented calcified deposition in contrast to small-pore PLA-nano grafts. Particularly, prolonged macrophage infiltration in the neointima of PLA-nano scaffolds may cause calcification, and regeneration of VSMCs may prevent calcification by sustaining a balance of osteogenesis and osteoclastogenesis in the neointima of tissue engineered arterial grafts during the remodeling process.

Conflict of interest

CB and TS receive grant support from Gunze Ltd.

CB receives grant support from Pall Corp (NY, USA).

ST and HK were recipients of Banyu Fellowship from Banyu Life Science Foundation International (Tokyo, Japan) (HK in 2011 and ST in 2012).

HK was recipient of fellowship from Shinsenkai Imabari Daiichi Hospital (Ehime, Japan) in 2013.

Acknowledgment

We acknowledge the excellent technical assistance of Yuki Sakamoto (Gunze Ltd), Hidetaka Nakayama (Gunze Ltd), and Paul S. Bagi (Yale University), and the advice of Toshio Matsumoto (Tokushima University). We would also like to thank Nancy Troiano, Rose Webb, and Christiane Coady of the Yale Core Center for Musculoskeletal Disorders for their technical expertise in processing murine TEVG tissue.

References

[1] Lim LS, Haq N, Mahmood S, Hoeksema L. Atherosclerotic cardiovascular disease screening in adults: American College of Preventive Medicine position statement on preventive practice. Am. J. Prev. Med. 2011;40(381):e1–10.
[2] Suma H. Arterial grafts in coronary bypass surgery. Ann. Thorac. Cardiovasc. Surg. 1999;5:141–5.
[3] Ravi S, Chaikof EL. Biomaterials for vascular tissue engineering. Regen. Med. 2010;5:107–20.
[4] Kannan RY, Salacinski HJ, Butler PE, Hamilton G, Seifalian AM. Current status of prosthetic bypass grafts: a review. J. Biomed. Mater. Res. B Appl. Biomater. 2005;74:570–81.
[5] Vacanti JP, Langer R. Tissue engineering: the design and fabrication of living replacement devices for surgical reconstruction and transplantation. Lancet 1999;354(Suppl. 1):SI32–4.
[6] Tara S, Rocco KA, Hibino N, et al. Vessel bioengineering. Circ. J. 2013;78:12–9.
[7] Roh JD, Nelson GN, Brennan MP, et al. Small-diameter biodegradable scaffolds for functional vascular tissue engineering in the mouse model. Biomaterials 2008;29:1454–63.
[8] Mirensky TL, Hibino N, Sawh-Martinez RF, et al. Tissue-engineered vascular grafts: does cell seeding matter? J. Pediatr. Surg. 2010;45:1299–305.
[9] Tara S, Kurobe H, Maxfield MW, et al. Evaluation of remodeling process in small-diameter cell-free tissue-engineered arterial graft. J. Vasc. Surg. 2014 (in press).
[10] Thompson B, Towler DA. Arterial calcification and bone physiology: role of the bone-vascular axis. Nat. Rev. Endocrinol. 2012;8:529–43.
[11] Wu M, Rementer C, Giachelli CM. Vascular calcification: an update on mechanisms and challenges in treatment. Calcif. Tissue Int. 2013;93:365–73.
[12] de Valence S, Tille JC, Mugnai D, et al. Long term performance of polycaprolactone vascular grafts in a rat abdominal aorta replacement model. Biomaterials 2012;33:38–47.
[13] Athanasiou KA, Niederauer GG, Agrawal CM. Sterilization, toxicity, biocompatibility and clinical applications of polylactic acid/polyglycolic acid copolymers. Biomaterials 1996;17:93–102.
[14] Li WJ, Laurencin CT, Caterson EJ, Tuan RS, Ko FK. Electrospun nanofibrous structure: a novel scaffold for tissue engineering. J. Biomed. Mater. Res. 2002;60:613–21.
[15] Wu H, Fan J, Chu CC, Wu J. Electrospinning of small diameter 3-D nanofibrous tubular scaffolds with controllable nanofiber orientations for vascular grafts. J. Mater. Sci. Mater. Med. 2010;21:3207–15.
[16] Drilling S, Gaumer J, Lannutti J. Fabrication of burst pressure competent vascular grafts via electrospinning: effects of microstructure. J. Biomed. Mater. Res. A 2009;88:923–34.
[17] Pektok E, Nottelet B, Tille JC, et al. Degradation and healing characteristics of small-diameter poly(epsilon-caprolactone) vascular grafts in the rat systemic arterial circulation. Circulation 2008;118:2563–70.
[18] Kuwabara F, Narita Y, Yamawaki-Ogata A, et al. Long-term results of tissue-engineered small-caliber vascular grafts in a rat carotid arterial replacement model. J. Artif. Organs 2012;15:399–405.
[19] Mrowczynski W, Mugnai D, de Valence S, et al. Porcine carotid artery replacement with biodegradable electrospun poly-e-caprolactone vascular prosthesis. J. Vasc. Surg. 2014;59:210–9.
[20] Sung HJ, Meredith C, Johnson C, Galis ZS. The effect of scaffold degradation rate on three-dimensional cell growth and angiogenesis. Biomaterials 2004;25:5735–42.
[21] Wu W, Allen RA, Wang Y. Fast-degrading elastomer enables rapid remodeling of a cell-free synthetic graft into a neoartery. Nat. Med. 2012;18:1148–53.
[22] Rocco KA, Maxfield MW, Best C, Dean EW, Breuer CK. In vivo applications of electrospun tissue-engineered vascular grafts: a review. Tissue Eng. B Rev. 2014 (in press).
[23] Hibino N, Yi T, Duncan DR, et al. A critical role for macrophages in neovessel formation and the development of stenosis in tissue-engineered vascular grafts. FASEB J. 2011;25:4253–63.
[24] Aikawa E, Nahrendorf M, Figueiredo JL, et al. Osteogenesis associates with inflammation in early-stage atherosclerosis evaluated by molecular imaging in vivo. Circulation 2007;116:2841–50.
[25] Speer MY, Yang HY, Brabb T, et al. Smooth muscle cells give rise to osteochondrogenic precursors and chondrocytes in calcifying arteries. Circ. Res. 2009;104:733–41.
[26] Sun Y, Byon CH, Yuan K, et al. Smooth muscle cell-specific runx2 deficiency inhibits vascular calcification. Circ. Res. 2012;111:543–52.
[27] Steitz SA, Speer MY, Curinga G, et al. Smooth muscle cell phenotypic transition associated with calcification: upregulation of Cbfa1 and downregulation of smooth muscle lineage markers. Circ. Res. 2001;89:1147–54.
[28] Doherty TM, Uzui H, Fitzpatrick LA, et al. Rationale for the role of osteoclast-like cells in arterial calcification. FASEB J. 2002;16:577–82.
[29] Byon CH, Sun Y, Chen J, et al. Runx2-upregulated receptor activator of nuclear factor kappaB ligand in calcifying smooth muscle cells promotes migration and osteoclastic differentiation of macrophages. Arterioscler. Thromb. Vasc. Biol. 2011;31:1387–96.

Evaluation of remodeling process in small-diameter cell-free tissue-engineered arterial graft

Shuhei Tara, MD, PhD,[a] Hirotsugu Kurobe, MD, PhD,[a] Mark W. Maxfield, MD,[b] Kevin A. Rocco, MS,[b] Tai Yi, MD,[a] Yuji Naito, MD, PhD,[b] Christopher K. Breuer, MD,[a] and Toshiharu Shinoka, MD, PhD,[a]
Columbus, Ohio; and New Haven, Conn

Objective: Autologous grafts are used to repair atherosclerotic cardiovascular diseases; however, many patients lack suitable donor graft tissue. Recently, tissue engineering techniques have emerged to make biologically active blood vessels. We applied this technique to produce arterial grafts using established biodegradable materials without cell seeding. The grafts were evaluated in vivo for vessel remodeling during 12 months.
Methods: Poly(L-lactide-co-ε-caprolactone) scaffolds reinforced by poly(lactic acid) (PLA) fiber were prepared as arterial grafts. Twenty-eight cell-free grafts were implanted as infrarenal aortic interposition grafts in 8-week-old female SCID/Bg mice. Serial ultrasound and micro computed tomography angiography were used to monitor grafts after implantation. Five grafts were harvested for histologic assessments and reverse transcription-quantitative polymerase chain reaction analysis at time points ranging from 4 months to 1 year after implantation.
Results: Micro computed tomography indicated that most implanted mice displayed aneurysmal changes (three of five mice at 4 months, four of five mice at 8 months, and two of five mice at 12 months). Histologic assessments demonstrated extensive tissue remodeling leading to the development of well-circumscribed neovessels with an endothelial inner lining, a neointima containing smooth muscle cells and elastin, and a collagen-rich extracellular matrix. There were a few observed calcified deposits, located around residual PLA fibers at 12 months after implantation. Macrophage infiltration into the scaffold, as evaluated by F4/80 immunohistochemical staining, remained after 12 months and was focused mostly around residual PLA fibers. Reverse transcription-quantitative polymerase chain reaction analysis revealed that gene expression of Itgam, a marker for macrophages, and of matrix metalloproteinase 9 was higher than in native aorta during the course of 12 months, indicating prolonged inflammation (Itgam at 8 months: 11.75 ± 0.99 vs native aorta, $P < .01$; matrix metalloproteinase 9 at 4 months: 4.35 ± 3.05 vs native aorta, $P < .05$).
Conclusions: In this study, we demonstrated well-organized neotissue of cell-free biodegradable arterial grafts. Although most grafts experienced aneurysmal change, such findings provide insight into the process of tissue-engineered vascular graft remodeling and should allow informed rational design of the next generation of arterial grafts. (J Vasc Surg 2014;■:1-10.)

Clinical Relevance: Tissue-engineered vascular grafts (TEVGs) hold promise for correcting some types of congenital heart disease because they are biocompatible, are antithrombogenic, and possess the capacity for growth. Recently, some studies showed the feasibility of TEVG for arterial graft using animal models. The aim of this study was to evaluate and to characterize the tissue remodeling process of one such TEVG made from clinically approved biodegradable materials. In this study, we report a highly patent TEVG featuring organized neotissue but that had some instances of aneurysmal change. These findings provide insight into the TEVG remodeling process and enable better design of next-generation arterial grafts.

Atherosclerotic cardiovascular disease (CVD) is a systemic narrowing and hardening of the arteries and includes conditions such as coronary heart disease, carotid artery stenosis, and peripheral arterial disease. CVD affects millions of patients and is the leading cause of morbidity and mortality in the United States.[1] Surgical intervention using autologous arterial and venous grafts is the most common corrective procedure for CVD; however, many patients lack suitable donor tissue because of previous surgery or as a result of their underlying vascular disease. Alternative synthetic grafts, such as expanded polytetrafluoroethylene (Gore-Tex) and polyethylene terephthalate (Dacron), have a history of long-term success when they are placed in large arteries whose flow is high and resistance low. However, current synthetic small-diameter (<6 mm) grafts are prone to occlusion by thrombogenesis and as a result are contraindicated. Synthetic materials have several other drawbacks, including risk of infection, persistent inflammation, calcification, and chronic need for anticoagulant therapy.

To address these challenges, tissue engineering techniques have emerged to make biologically active blood

From the Tissue Engineering Program and Surgical Research, Nationwide Children's Hospital, Columbus[a]; and the Department of Surgery, Yale University School of Medicine, New Haven.[b]

Author conflict of interest: C.K.B. and T.S. receive grant support from Gunze Ltd and the Pall Corp; this funding was not used to support the work described in this manuscript. H.K. (in 2011) and S.T. (in 2012) were recipients of the Banyu Fellowship from Banyu Life Science Foundation International (Tokyo, Japan). H.K. (in 2013) was recipient of a fellowship from Shinsenkai Imabari Daiichi Hospital (Ehime, Japan).

Reprint requests: Toshiharu Shinoka, MD, PhD, 700 Children's Dr, Columbus, OH 43205 (e-mail: toshiharu.shinoka@nationwidechildrens.org).

The editors and reviewers of this article have no relevant financial relationships to disclose per the JVS policy that requires reviewers to decline review of any manuscript for which they may have a conflict of interest.
0741-5214/$36.00

http://dx.doi.org/10.1016/j.jvs.2014.03.011

vessels, called tissue-engineered vascular grafts (TEVGs). The traditional concept of tissue engineering consists of the following three components: (1) a tissue-inducing scaffold material, (2) the isolation and use of cells or cell substitutes, and (3) the integration of the cells and the scaffold by a seeding technique.[2] We have successfully applied this technique in a low-pressure environment (<30 mm Hg)[3] and have performed TEVG implantation in 25 pediatric patients in Japan.[4] Currently, we have begun a clinical trial in the United States with approval of the Food and Drug Administration (FDA) for implantation of TEVGs in patients undergoing extracardiac total cavopulmonary connection procedures. To achieve this, we employ highly porous, biodegradable grafts composed of poly(L-lactide-co-ε-caprolactone) (PLCL) reinforced by mesh of poly(glycolic acid) that are seeded with bone marrow-derived mononuclear cells. As the synthetic scaffolding degrades away, a new blood vessel is formed in its place by the infiltration of the host's own smooth muscle cells and endothelial cells from the adjacent native blood vessel.

For the TEVG strategy to be translated to arterial applications, the graft must withstand arterial pressures while maintaining sufficient porosity for cellular infiltration. Moving toward that reality, we confirmed the feasibility of TEVGs with and without cell seeding in a small-diameter arterial model.[5,6] Furthermore, several groups have also demonstrated different types of TEVGs without cell seeding for small-diameter arterial grafts.[7,8] The electrospinning technique, which enables the production of nanofiber-based scaffolds, has been proposed as a promising technique for fabrication of arterial TEVGs[9] and has shown good surgical and mechanical properties with a high patency rate in an arterial implantation model.[10] However, we believe that cellular migration into the scaffold was likely inhibited by the tightly knitted nanofiber, causing prolonged neotissue remodeling and foreign body reaction. Moving forward, we created a cell-free TEVG for arterial circulation constructed from PLCL and reinforced by poly(lactic acid) (PLA) fiber mesh (PLA-PLCL grafts) to enhance cell migration into the scaffold. Herein, we used the PLA-PLCL grafts to evaluate the process of vessel remodeling with implantation in a mouse abdominal aorta model during a 12-month period.

METHODS

Animals. All animals received humane care in compliance with the National Institutes of Health *Guide for the Care and Use of Laboratory Animals.* The Institutional Animal Care and Use Committee at Yale University approved the use of animals and all procedures described in this study. The 8-week old female SCID/Bg mice were purchased from Jackson Laboratories (Bar Harbor, Me).

Scaffolds. PLA-PLCL grafts were constructed with use of a dual-cylinder chamber molding system from a nonwoven 100% PLA fiber mesh (molecular weight, 120,000; Biomedical Structures, Warwick, RI) and a 50:50 PLCL (molecular weight, 360,000; Gunze Co, Ltd, Kyoto, Japan) sealant solution on the basis of conventional grafts previously described.[6] Pore size of the scaffold was about 30 μm, and wall thickness was about 250 μm. Wall thickness changed over time according to tissue remodeling. Each scaffold was 3 mm in length, and inner luminal diameters were between 500 and 600 μm (Fig 1, *A*). All scaffolds were sterilized by overnight ultraviolet radiation preceding implantation.

Graft implantation. Twenty-eight grafts were implanted as infrarenal aortic interposition conduits with a running 10-0 nylon suture for the end-to-end proximal and distal anastomoses by standard microsurgical technique (Fig 1, *B*). Details of the method for graft implantation were described in our previous report.[5] Neither antiplatelet nor anticoagulant agents were used during aortic cross-clamping or the perioperative period in this study. Because we observed an entirely equivalent model with the same graft for 6 weeks in our previous study,[6] we decided the time point for evaluation of late-term tissue remodeling to be 4, 8, and 12 months. Five mice were selected randomly and sacrificed at each time point, and harvested grafts were separated in half for different analysis.

Twelve sham operations were performed (opening and closing of the abdomen with exposure of the aorta) to evaluate the natural causes of aortic disease, such as aortic calcification and dilation, for 12 months.

Ultrasound. Serial ultrasonography (Vevo Visualsonics 770; Visualsonics, Toronto, Ontario, Canada) was used to serially monitor grafts after implantation. Before ultrasonography, mice were anesthetized with 1.5% inhaled isoflurane.

Contrast-enhanced micro computed tomography (CT) angiography. We selected five mice at each time point randomly, and in vivo micro CT angiography was performed under anesthesia with the GE eXplore Locus in vivo micro CT scanner (GE Healthcare, Milwaukee, Wisc). One minute before image acquisition, animals were given an intrajugular 0.3 mL bolus of Ultravist (370 mg I/mL; Bayer Healthcare, Wayne, NJ). Micro CT data were transferred to the Advanced Workstation (version 4.4; GE Healthcare) for further reconstruction and quantitative analysis. Measurements of graft length, inner luminal diameter, and graft volume were performed. Similar measurements were obtained in controls having undergone sham operation.

Histology and immunohistochemistry. Explanted grafts at 4, 8, and 12 months after implantation and native abdominal aortas were fixed in 4% paraformaldehyde and embedded in paraffin. Sections 5 μm thick were then stained by standardized techniques for hematoxylin and eosin, Masson trichrome, elastica-van Gieson, and von Kossa.

Identification of endothelial cells, smooth muscle cells, macrophages, and matrix metalloproteinase 2 (MMP-2) was done by immunohistochemical staining of paraffin-embedded explant sections with rabbit anti-CD31 (1:50; Abcam, Cambridge, Mass), mouse anti-smooth muscle actin (1:500; Dako, Carpinteria, Calif), rat anti-F4/80 (1:1000; AbD Serotec, Oxford, UK), and rabbit anti-MMP-2

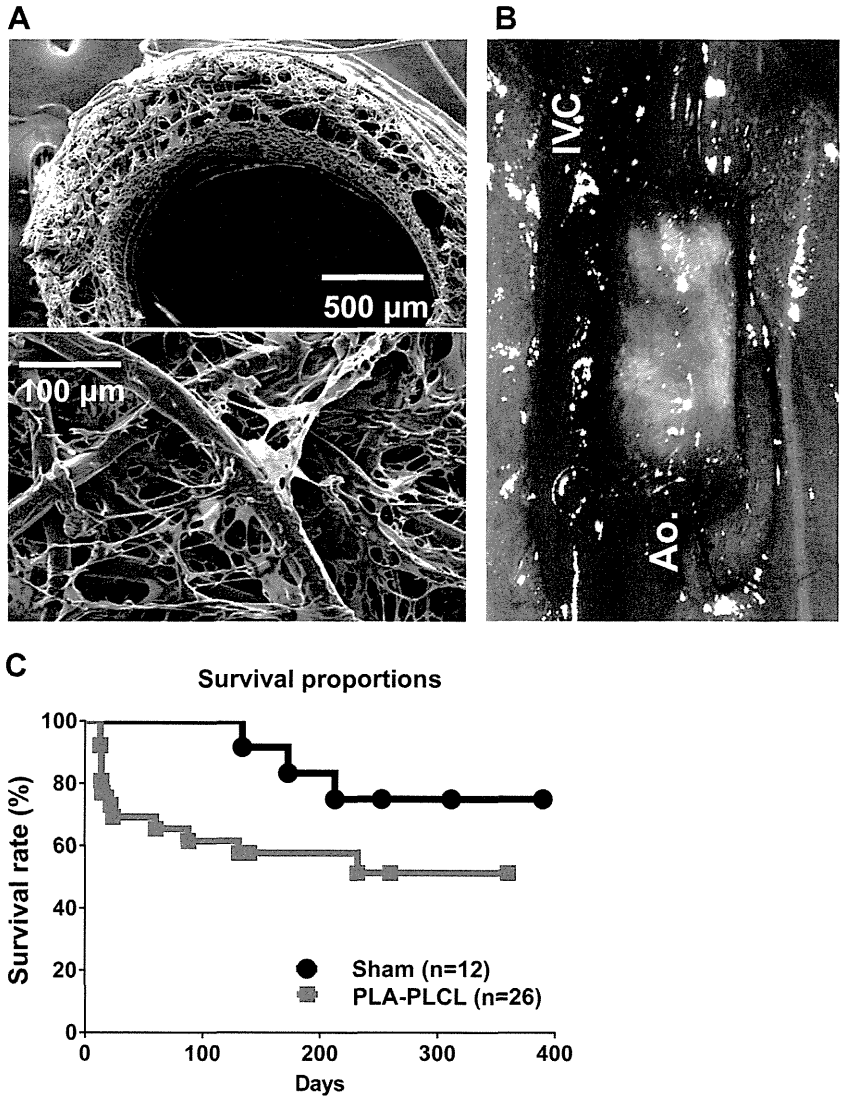

Fig 1. A, Scanning electron microscopy image of biodegradable scaffold, with porous microstructure allowing cellular infiltration. **B,** Intraoperative photograph demonstrating tissue-engineered vascular graft during surgical implantation. *Ao,* Aorta; *IVC,* inferior vena cava. **C,** Survival proportions during follow-up period of poly(lactic acid)-poly(L-lactide-co-ε-caprolactone) (*PLA-PLCL*) graft group compared with sham group.

(1:500; Abcam), respectively. Primary antibody binding was detected with biotinylated goat anti-rat immunoglobulin G (1:200; Vector, Burlingame, Calif), biotinylated goat anti-rabbit immunoglobulin G (1:200; Vector), and biotinylated goat anti-mouse immunoglobulin G (1:200; Vector), respectively. This was followed by the binding of streptavidin–horseradish peroxidase and color development with 3,3-diaminobenzidine.

RNA extraction and reverse transcription-quantitative polymerase chain reaction (RT-qPCR). Explanted grafts at 4, 8, and 12 months after implantation and native abdominal aortas were frozen in optimal cutting temperature (OCT) compound (Tissue-Tek; Sakura Finetek, Torrance, Calif) and sectioned into 20 sections of 30 μm with a Leica CM 1950 cryostat (Leica Biosystems, Wetzlar, Germany). Excess OCT compound was removed by centrifugation in phosphate-buffered saline. Total RNA was extracted and purified by the RNeasy Mini Kit (Qiagen, Venlo, The Netherlands) according to the manufacturer's instructions. Reverse transcription was performed with a High Capacity RNA-to-cDNA Kit (Applied Biosystems, Carlsbad, Calif). All reagents and instrumentation for gene expression analysis were obtained from Applied Biosystems. RT-qPCR was performed with a StepOnePlus Real-Time PCR System using the TaqMan Universal PCR Master Mix Kit. Reference numbers for primers are as follows: collagen type I (Col1a1; Mm00801666_g1), collagen type III (Col3a1; Mm01254476_m1), elastin (Eln; Mm00514670_m1),

vimentin (vim; Mm01333430_m1), integrin alpha M (Itgam; Mm00434455_m1), matrix metallopeptidase 2 (MMP-2; Mm00439498_m1), matrix metallopeptidase 9 (MMP-9; Mm00442991_m1), transforming growth factor β1 (TGF-β1; Mm01178820_m1), and hypoxanthine-guanine phosphoribosyltransferase (HPRT; Mm00446968_m1). The results were analyzed with the comparative threshold cycle method and normalized with HPRT as an endogenous reference and reported as relative values (ΔΔ CT) to those of control native aorta.

Statistical analysis. To decide the sample number, a power calculation by log-rank test with .05 of α error and .8 of power was completed. We estimated that the event-free survival rate at the time point of 12 months after the implantation was 0.98 for the sham operation group and 0.3 for the PLA-PLCL implantation group. Results are expressed as mean ± standard deviation, and the number of experiments is shown in each case. Data for RT-qPCR were statistically analyzed by one-way analysis of variance followed by Tukey HSD. A probability value of less than .05 was considered statistically significant. All statistical analysis was done with SPSS (version 20; IBM, Armonk, NY).

RESULTS

Microsurgical implantation of tissue-engineered vascular grafts in mice as infrarenal interposition aortic conduits. Twenty-eight PLA-PLCL grafts were implanted as infrarenal interposition aortic conduits, and 12 syngeneic mice underwent sham operations. Perioperative survival was 92.9% in the PLA-PLCL graft group and 100% in the sham group. The survival rate of the remaining 26 mice in the PLA-PLCL graft group was 53.8% at 12 months (sham group, 75.0%) (Fig 1, *C*). Twelve mice from the PLA-PLCL graft group died of graft rupture, and three mice of the sham group died of undetermined causes. These were confirmed by autopsy within 24 hours after death.

Serial ultrasonographic imaging demonstrated luminal patency and laminar flow in all grafts through 12 months. Implanted grafts were serially monitored by ultrasound to assess for both patency and aneurysm. Doppler ultrasound detected normal blood flow at the proximal and distal ends of the implanted grafts and also within each graft (Fig 2, *A*). The images of implanted PLA-PLCL grafts with and without aneurysmal change are shown in Fig 2, *B*.

Assessment of graft morphometry by micro CT angiography demonstrated dilation to 12 months after implantation. In vivo micro CT angiography was performed at months 4 (n = 5), 8 (n = 5), and 12 (n = 5). Age-matched controls were also analyzed at each time point (n = 2-3 in each point). Most implanted mice had evidence of aortic dilation including aneurysmal change (three of five mice at 4 months, four of five mice at 8 months, and two of five mice at 12 months; Fig 2, *C*).

Luminal volume calculations with a standard graft length of 3 mm were as follows: native aorta, 0.8 ± 0.08 mm^3; PLA-PLCL graft, 2.3 ± 0.7 mm^3 at 4 months, 2.7 ± 0.6 mm^3 at 8 months, and 2.0 ± 0.8 mm^3 at 12 months (Fig 2, *D*).

Histologic assessment and RT-qPCR demonstrated cellular infiltration and neovessel remodeling. Histologic assessment demonstrated cell infiltration within the scaffolding as early as 4 months after implantation with a concomitant neointima (Fig 3, *A*). However, abundant PLA fibers, which may appear as vacuoles or capillaries, still existed in the scaffold layer at 12 months after implantation. Although the neointimal layer progressively augmented in thickness during the course of 12 months, the inner surface of this layer was covered by a confluent monolayer of endothelial cells (Fig 3, *B*).

Extracellular matrix (ECM) is the primary determinant of the biomechanical properties of neovessel. Consequently, we evaluated ECM components including collagen and elastin by histology and RT-qPCR. Although PLA fiber remained at 12 months, Masson trichrome staining showed a gradual increase in deposition of collagen within the polymer scaffolding (Fig 4, *A*). These qualitative assessments were quantitatively confirmed with gene expression by RT-qPCR. Collagen type I increased during the course of 12 months and collagen type III peaked at 8 months, and these levels were significantly higher than those of native aorta (collagen type I at 12 months: 4.69 ± 1.57 vs native aorta, $P < .001$; collagen type III at 8 months: 2.30 ± 0.38 vs native aorta, $P < .01$; Fig 4, *B*). Although elastin deposition within the neointimal layer was shown on elastica-van Gieson staining (Fig 4, *A*), gene expression of elastin in the PLA-PLCL graft was lower than that in native aorta (8 months: 0.33 ± 0.05 vs native aorta, $P < .05$; Fig 4, *B*).

Smooth muscle cells are the predominant cells in the arterial wall and are essential for the structural and functional integrity of the neovessel. In the present study, smooth muscle cells, which were defined by immunohistochemical smooth muscle actin staining, were shown at 8 months in the neointima and augmented at 12 months after implantation (Fig 4, *A*). Last, gene expression of vimentin, a mesenchymal cell marker, increased during the course of 12 months (12 months: 3.64 ± 0.86 vs native aorta, $P < .001$; Fig 4, *B*).

We were not able to collect data comparing the neotissue components between aneurysmal and nonaneurysmal grafts.

Macrophage infiltration and MMP activity in neotissue were elevated during the course of 12 months after implantation. Previously, we demonstrated that TEVGs transformed into functional neovessels by an inflammatory process of vascular remodeling,[11] and macrophages have been shown to play critical roles in this process.[12] MMPs degrade structural components within the ECM, and MMP-2 and MMP-9 were shown to be involved in the remodeling process of TEVGs.[13]

In this study, macrophage infiltration into scaffold, evaluated by F4/80 immunohistochemical staining, remained at 12 months, localized around the remaining

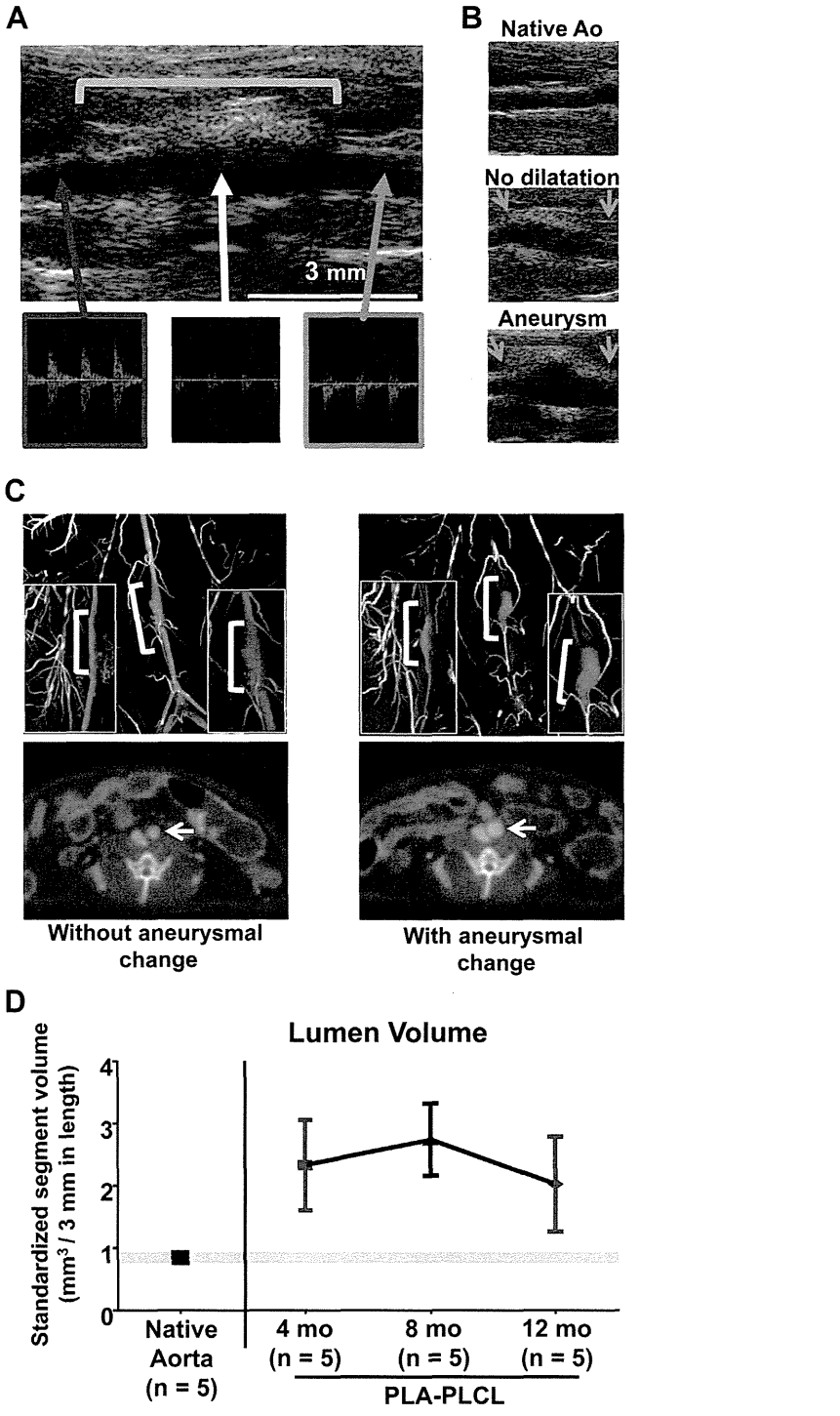

Fig 2. A, Serial Doppler ultrasound examinations were performed on poly(lactic acid)-poly(L-lactide-co-ε-caprolactone) (*PLA-PLCL*) grafts. All grafts remained patent to the experimental end point. **B,** Ultrasound images of no dilation and aneurysm of PLA-PLCL graft compared with native abdominal aorta (*Ao*). The *arrows* indicate the anastomoses. **C,** In vivo micro computed tomography (CT) angiography (n = 5/each time point) was performed at 4, 8, and 12 months. *Yellow bar* indicates approximate location of PLA-PLCL graft in a three-dimensional reconstructed micro CT image. The *arrows* in cross-sectional micro CT images indicate the implanted graft. **D,** Luminal volume was calculated by micro CT image processing software. Graft luminal volumes were standardized to a 3-mm segment.

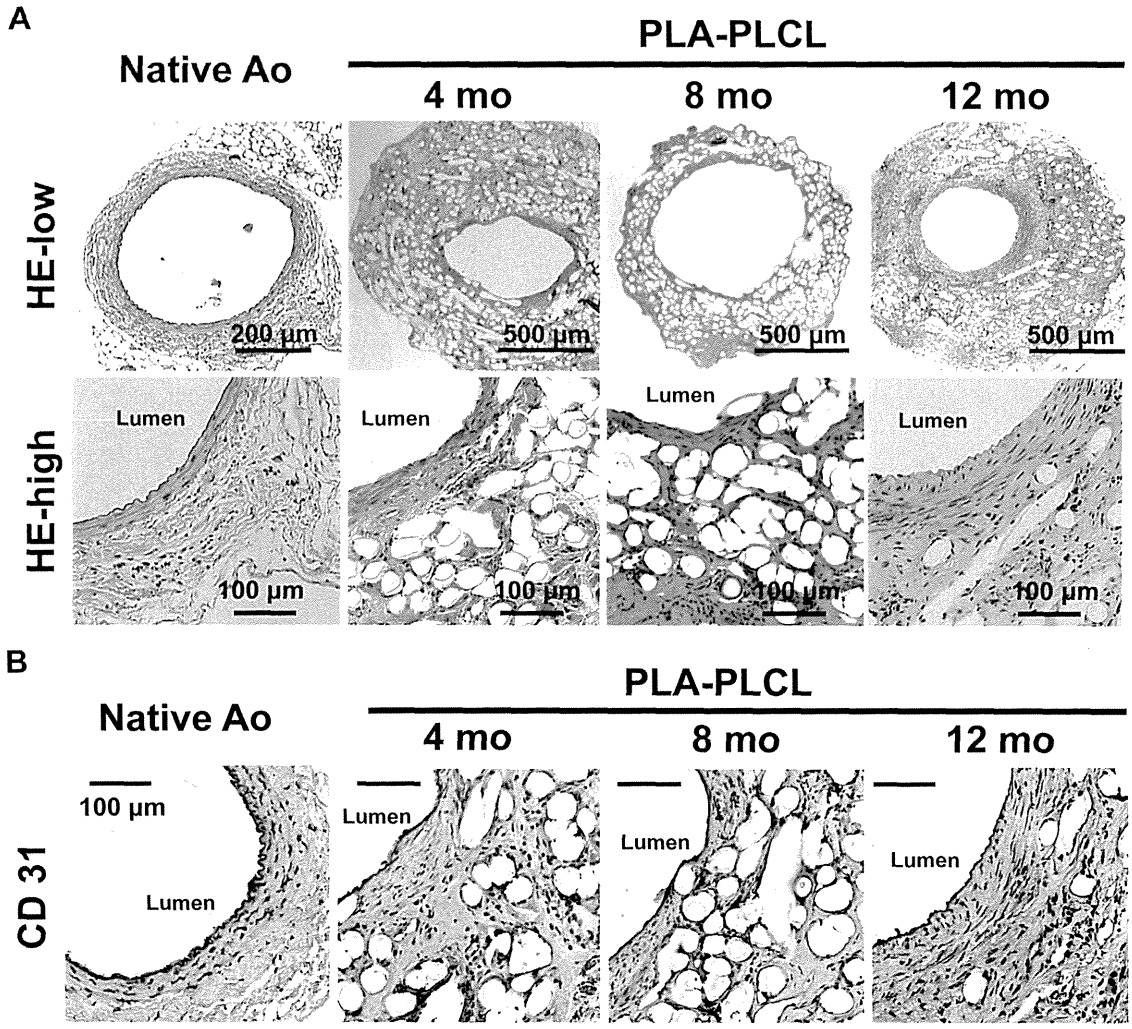

Fig 3. Representative histologic image of **(A)** hematoxylin and eosin (*HE*) staining with low- and high-power magnifications and **(B)** CD31 immunohistochemical staining. Grafts at 4, 8, and 12 months after implantation and native abdominal aortas were explanted, and formalin-fixed paraffin-embedded 5-μm cross sections were stained with HE or endothelial cell marker CD31 primary antibody at each time point and analyzed for cell infiltration and an endothelial layer, respectively. *Ao*, Aorta; *PLA-PLCL*, poly(lactic acid)-poly(L-lactide-co-ε-caprolactone).

PLA polymer fibers (Fig 5, *A*). Sustained elevation of MMP-2 activity was observed at each time point and exclusively at the interface between the graft layer and the intimal layer at 12 months (Fig 5, *A*). RT-qPCR analysis revealed that gene expression of Itgam for macrophage marker, MMP-2, and MMP-9 was higher than in native aorta (Itgam at 8 months: 11.75 ± 0.99 vs native aorta, $P < .01$; MMP-2 at 8 months: 2.68 ± 0.41 vs native aorta, $P < .05$; MMP-9 at 4 months: 4.35 ± 3.05 vs native aorta, $P < .05$; Fig 5, *B*).

TGF-β1 has been shown to play an important role in tissue repair as it is a key regulator of the production and remodeling of the ECM through its effect on mesenchymal cells.[14] For evaluation of the ongoing neovessel remodeling, the gene expression of TGF-β1 was measured and shown to be higher in TEVGs than in native aorta at each time point, indicating an active and ongoing remodeling process throughout the 12 months (12 months: 3.45 ± 0.52 vs native aorta, $P < .001$; Fig 5, *B*).

Calcific deposition in neotissue. During the course of neovessel remodeling, these implants are susceptible to calcification, a potentially fatal problem in a long-term application. von Kossa staining showed that there was no calcification in the neointimal layer at all during the course of 12 months, although a little calcification was observed around the remaining PLA fiber (Fig 5, *A*).

DISCUSSION

In this study, we used a mouse aortic implantation model with a cell-free PLCL scaffold reinforced by PLA

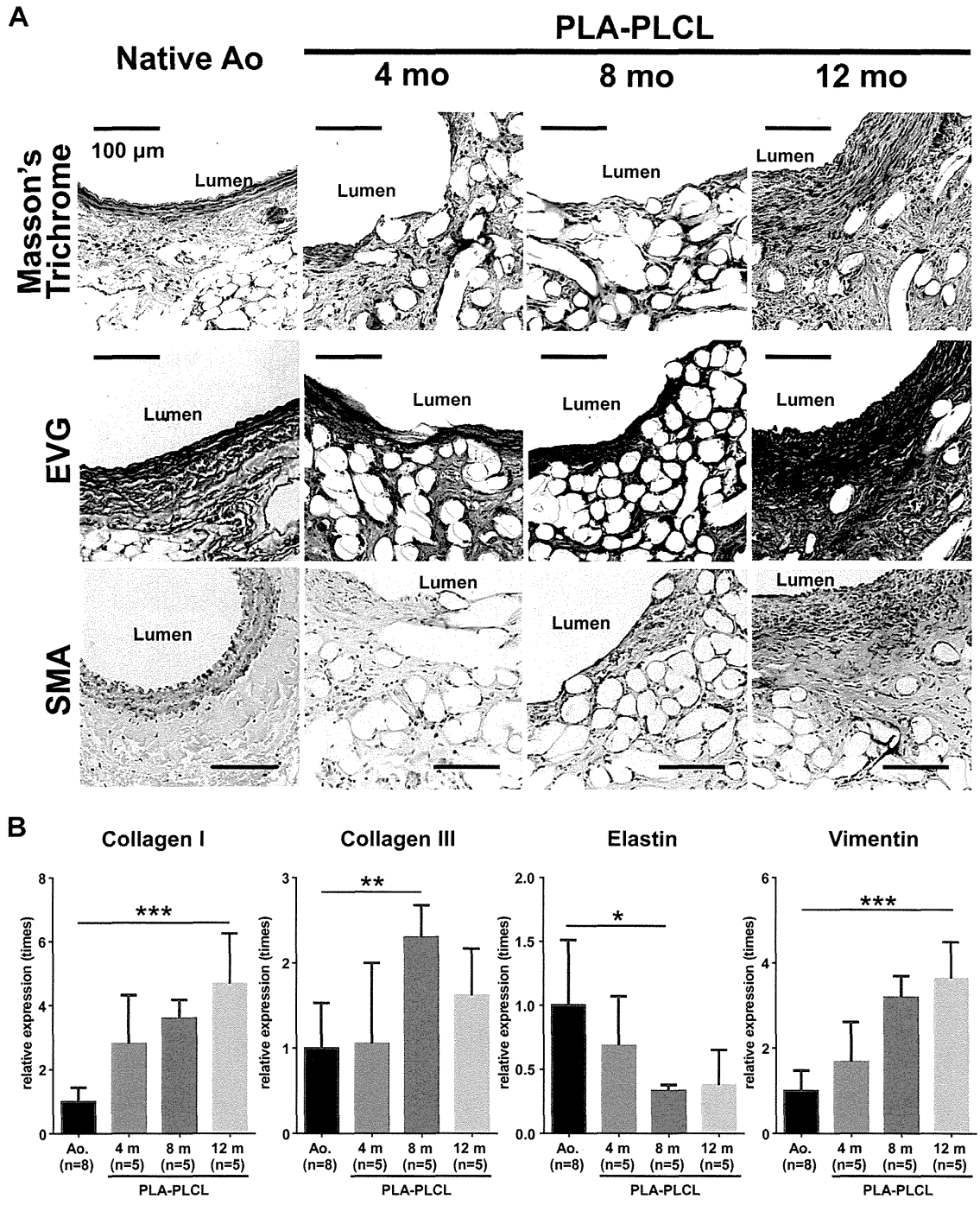

Fig 4. Neotissue formation of poly(lactic acid)-poly(L-lactide-co-ε-caprolactone) (*PLA-PLCL*) graft. Collagen and elastin deposition in neovessels was evaluated by histology and reverse transcription-quantitative polymerase chain reaction (RT-qPCR). **A,** Representative histologic image of Masson trichrome staining for collagen deposition, elastica-van Gieson (*EVG*) staining for elastic formation, and immunohistochemical smooth muscle actin (*SMA*) staining for smooth muscle cells within the neointima at 4, 8, and 12 months after implantation. *Ao*, Aorta. **B,** Gene expression of eight native aortas (control) and five grafts at each time point was analyzed by RT-qPCR with the ΔΔ CT method. Vimentin was used as a marker of mesenchymal cells including smooth muscle cells. Data are expressed as fold change over native aorta expression (mean ± standard deviation; $*P < .05$, $**P < .01$, $***P < .001$).

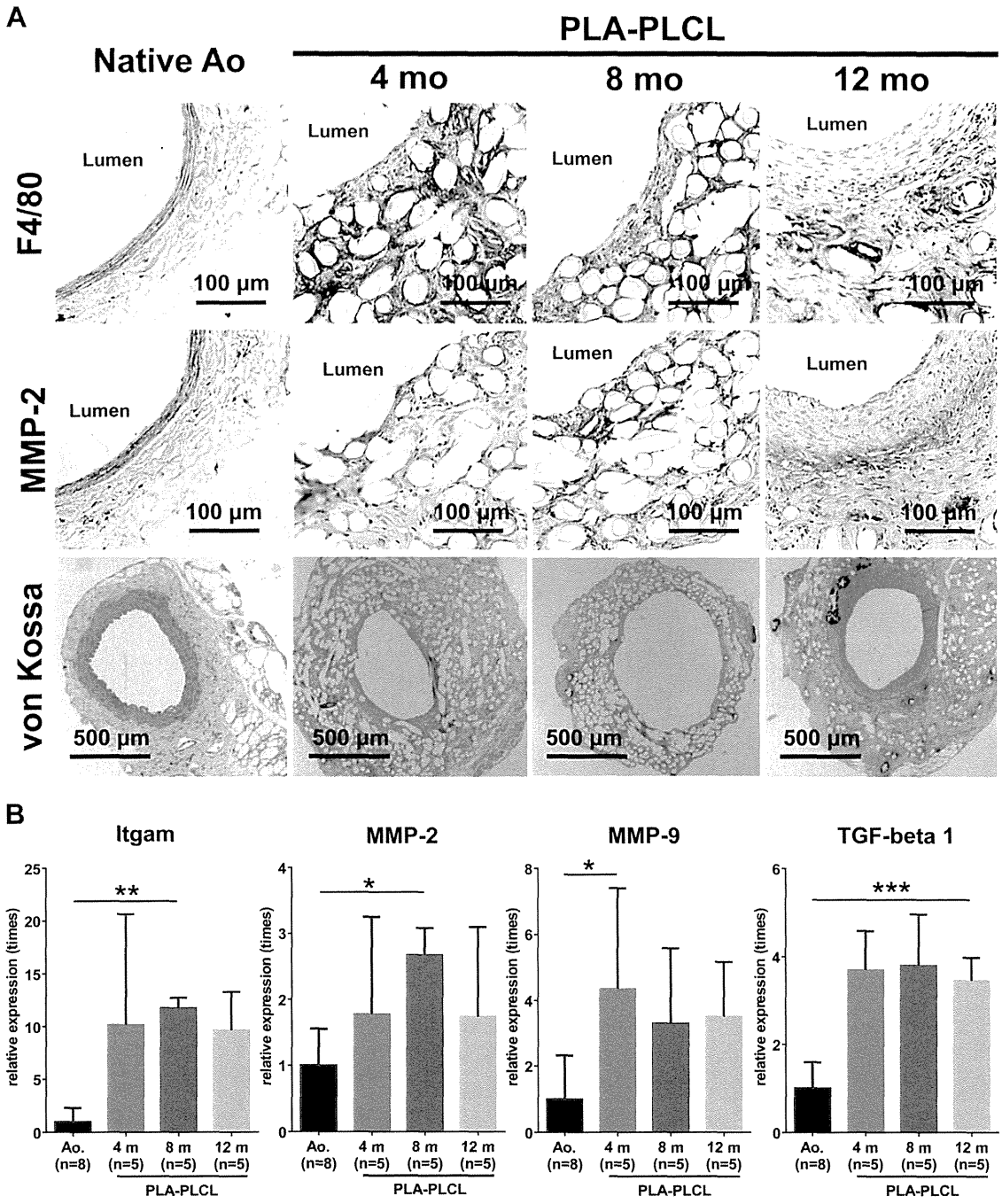

Fig 5. Inflammatory process and calcification of poly(lactic acid)-poly(L-lactide-co-ε-caprolactone) (*PLA-PLCL*) graft. Macrophage infiltration and matrix metalloproteinase (*MMP*) activity in neotissue were evaluated by immunohistochemical staining and reverse transcription-quantitative polymerase chain reaction (RT-qPCR). Calcification in neotissue was evaluated by von Kossa staining. **A,** Representative images of immunohistochemical stainings of macrophage marker F4/80 and MMP-2 and von Kossa staining at 4, 8, and 12 months after implantation. *Ao,* Aorta. **B,** Gene expression of eight native aortas (control) and five grafts at each time point was analyzed by RT-qPCR with the ΔΔ CT method. Itgam was used as a macrophage marker. Data are expressed as fold change over native aorta expression (mean ± standard deviation; $*P < .05$, $**P < .01$, $***P < .001$). *TGF,* Transforming growth factor.

fiber mesh as a biodegradable arterial TEVG. Advantages of the present investigation, compared with previous studies,[7-10] are that these materials are commonly used for constructing TEVGs because of their history of successful clinical application, are FDA approved for human implantation, and possess a broad range of material properties.[15] The construction of our graft in this study is comparable to the TEVG for inferior vena cava implantation that is already accepted for use in a clinical trial in the United States.[16] Furthermore, we observed this model for 12 months.

Neovessel formation is a dynamic process characterized by progressive degradation of the scaffold due to hydrolysis, cellular infiltration into the scaffold, and ECM deposition. The degradation period of our PLCL is approximately 4 to 6 weeks and that of PLA is more than 1 year.[6] The basic concept of our graft is to induce neovessel remodeling according to the degradation of PLCL while providing reinforcement by the PLA fiber mesh even after the disappearance of PLCL. Our study showed that 4 months after implantation, the PLCL was completely degraded with robust cellular infiltration, while PLA fibers still remained at 12 months. The neovessel demonstrated progressive remodeling, leading to the development of well-circumscribed tissue with an endothelial inner lining and a neointima containing collagens, elastin, and smooth muscle cells, although we did not collect data analyzing the function of these cells.

Whereas the present model of the arterial graft can achieve our basic TEVG strategy, most grafts experienced dilation or aneurysmal change from the first time point (4 months). Previously, we observed no aneurysm of the same arterial PLA-PLCL graft until 6 weeks after implantation.[6] These findings indicate that aneurysmal degeneration of PLA-PLCL began between 6 weeks and 4 months after implantation. The purported mechanism of aneurysmal degeneration of the graft is that neotissue formation in the scaffold was not enough to endure arterial pressure during the course of PLA degradation. Furthermore, continuous inflammation and MMP activity might be involved in this process. To solve this issue, TEVG design may require two approaches, including stronger reinforcement, such as combinational use of electrospinning,[7-10] and improvement of cellular growth and ECM deposition in the scaffold. Heparin coating on TEVGs has the potential to facilitate cell infiltration into the scaffold as well as to decrease the risk of thrombosis,[7] and other cytokines may improve remodeling of TEVGs. Techniques of local cytokine release from the scaffold are another option for TEVGs to achieve "off-the shelf" availability.

The gene expression of elastin in our graft remained lower than that in native aorta, although elastica-van Gieson staining suggested the presence of elastin in the neointima as early as 4 months after implantation. The elastic matrix is responsible for providing vessels with the necessary compliance for systolic stretch.[17] In the present study, the elastin observed by histology might be either insufficient or less functional, considering our results that most of the implants displayed aneurysmal changes. The protein product of the elastin gene is synthesized by vascular smooth muscle cells and secreted as a tropoelastin monomer,[18] and its deposition was enhanced when stimulated by cyclic stretching.[19,20] In the present study, we speculate that mechanical stimulation of the smooth muscle cells by pulsatile stretching may have been limited by the residual PLA fibers, thereby reducing elastin production or function in the neoartery.

Histologic assessments indicated that macrophage infiltration into scaffold peaked at an early phase of neotissue formation, and smooth muscle cells were present 8 months after implantation. MMP activity was assessed by gene expression of MMP-9 and MMP-2. We found that MMP-9 expression peaked in the earlier phase of neovessel formation relative to that of MMP-2. MMP-9 is known as the most prominent type of MMP present in a foreign body inflammatory response,[21] and macrophage infiltration is promoted by MMP-9.[22] Consecutively, the migration of smooth muscle cells was shown to be dependent on MMP-2 and MMP-9.[22] MMP-2 is mainly produced by mesenchymal cells when stimulated by inflammatory cells.[23] In our previous study using a cell-seeded TEVG implanted into the mouse inferior vena cava, MMP-9 peaked at 1 week after implantation and decreased thereafter, although MMP-2 increased during the 4-week observation period.[13] These findings indicate that the process of foreign body reaction and tissue remodeling in the present arterial model is similar to our previous venous model but probably prolonged because of the remaining PLA fiber.

The results of this study showed that gene expression of TGF-β1 was higher than that of native aorta during the course of the observation period. TGF-β is a multifunctional cytokine that regulates cell proliferation, differentiation, adhesion, migration, and apoptosis.[24] TGF-β signaling plays an essential role in vascular remodeling, and its abnormality is known to cause vascular dysfunction such as aortic aneurysm.[24] Our previous study indicated that the PLA-PLCL graft possessed sufficient mechanical strength and properties to function as an arterial graft after testing of burst pressure, suture retention strength, Young modulus, and tensile strength and demonstrated no aneurysmal formation after short-term (6-week) follow-up.[6] On the basis of these findings, continuous elevation of TGF-β at later time points might induce the vascular dysfunction of our grafts followed by aneurysmal change. Interestingly, angiotensin receptor blockers are known to inhibit TGF-β signaling and to prevent aortic aneurysm in Marfan syndrome.[25,26] This drug may also have therapeutic potential to prevent aneurysmal change of the arterial TEVG in our model.

At the beginning of this study, we predicted thrombosis or occlusion of our PLA-PLCL graft with high frequency at the time point of 12 months because our previous short-term observation using wild-type C57BL/6 mice showed a high-frequency rate of these events. However, our present finding did not support this initial

hypothesis. One possible reason is that the SCID/Bg model may prevent thrombosis and neotissue hyperplasia of the PLA-PLCL graft. On the basis of this limitation, we have created an aortic implantation model in the wild-type C57BL/6 mouse without acute thrombosis by use of antiplatelet and anticoagulant drugs. Furthermore, vascular dysfunction followed by aneurysm may be caused even after complete scaffold degradation. Therefore, we must evaluate vascular function of arterial TEVGs with a model of long-term follow-up, such as in large animals.

CONCLUSIONS

We observed a cell-free PLA-PLCL graft for 12 months in a mouse aortic implantation model. Although well-organized neotissue was demonstrated, aneurysmal rupture was observed in 46% of implanted TEVGs. The concept of a cell-free arterial TEVG was partially proven in an arterial system with use of FDA-approval materials.

We acknowledge the excellent technical assistance of Cameron A. Best, Paul S. Bagi, and Zhen W. Zhuang. We would also like to thank Nancy Troiano, Rose Webb, and Christiane Coady of the Yale Core Center for Musculoskeletal Disorders for their technical expertise in processing murine TEVG tissue.

AUTHOR CONTRIBUTIONS

Conception and design: ST, HK, TS
Analysis and interpretation: ST, HK, MM, KR, TY, YN
Data collection: ST, HK, MM, KR, TY, YN
Writing the article: ST, HK
Critical revision of the article: ST, HK, CB, TS
Final approval of the article: ST, HK, MM, KR, TY, YN, CB, TS
Statistical analysis: ST, HK
Obtained funding: CB, TS
Overall responsibility: TS
ST and HK contributed equally to this article and share co-first authorship.

REFERENCES

1. Lim LS, Haq N, Mahmood S, Hocksema L. Atherosclerotic cardiovascular disease screening in adults: American College Of Preventive Medicine position statement on preventive practice. Am J Prev Med 2011;40:381.e1-e10.
2. Langer R, Vacanti JP. Tissue engineering. Science 1993;260:920-6.
3. Shin'oka T, Imai Y, Ikada Y. Transplantation of a tissue-engineered pulmonary artery. N Engl J Med 2001;344:532-3.
4. Hibino N, McGillicuddy E, Matsumura G, Ichihara Y, Naito Y, Breuer C, et al. Late-term results of tissue-engineered vascular grafts in humans. J Thorac Cardiovasc Surg 2010;139:431-6.
5. Mirensky TL, Nelson GN, Brennan MP, Roh JD, Hibino N, Yi T, et al. Tissue-engineered arterial grafts: long-term results after implantation in a small animal model. J Pediatr Surg 2009;44:1127-32.
6. Roh JD, Nelson GN, Brennan MP, Mirensky TL, Yi T, Hazlett TF, et al. Small-diameter biodegradable scaffolds for functional vascular tissue engineering in the mouse model. Biomaterials 2008;29:1454-63.
7. Wu W, Allen RA, Wang Y. Fast-degrading elastomer enables rapid remodeling of a cell-free synthetic graft into a neoartery. Nat Med 2012;18:1148-53.
8. Kuwabara F, Narita Y, Yamawaki-Ogata A, Satake M, Kaneko H, Oshima H, et al. Long-term results of tissue-engineered small-caliber vascular grafts in a rat carotid arterial replacement model. J Artif Organs 2012;15:399-405.
9. Mrowczynski W, Mugnai D, de Valence S, Tille JC, Khabiri E, Cikirikcioglu M, et al. Porcine carotid artery replacement with biodegradable electrospun poly-ε-caprolactone vascular prosthesis. J Vasc Surg 2014;59:210-9.
10. Wang S, Mo XM, Jiang BJ, Gao CJ, Wang HS, Zhuang YG, et al. Fabrication of small-diameter vascular scaffolds by heparin-bonded P(LLA-CL) composite nanofibers to improve graft patency. Int J Nanomedicine 2013;8:2131-9.
11. Roh JD, Sawh-Martinez R, Brennan MP, Jay SM, Devine L, Rao DA, et al. Tissue-engineered vascular grafts transform into mature blood vessels via an inflammation-mediated process of vascular remodeling. Proc Natl Acad Sci U S A 2010;107:4669-74.
12. Hibino N, Yi T, Duncan DR, Rathore A, Dean E, Naito Y, et al. A critical role for macrophages in neovessel formation and the development of stenosis in tissue-engineered vascular grafts. FASEB J 2011;25:4253-63.
13. Naito Y, Williams-Fritze M, Duncan DR, Church SN, Hibino N, Madri JA, et al. Characterization of the natural history of extracellular matrix production in tissue-engineered vascular grafts during neovessel formation. Cells Tissues Organs 2012;195:60-72.
14. Klass BR, Grobbelaar AO, Rolfe KJ. Transforming growth factor beta1 signalling, wound healing and repair: a multifunctional cytokine with clinical implications for wound repair, a delicate balance. Postgrad Med J 2009;85:9-14.
15. Athanasiou KA, Niederauer GG, Agrawal CM. Sterilization, toxicity, biocompatibility and clinical applications of polylactic acid/polyglycolic acid copolymers. Biomaterials 1996;17:93-102.
16. Shinoka T, Breuer C. Tissue-engineered blood vessels in pediatric cardiac surgery. Yale J Biol Med 2008;81:161-6.
17. Venkataraman L, Ramamurthi A. Induced elastic matrix deposition within three-dimensional collagen scaffolds. Tissue Eng Part A 2011;17:2879-89.
18. Patel A, Fine B, Sandig M, Mequanint K. Elastin biosynthesis: the missing link in tissue-engineered blood vessels. Cardiovasc Res 2006;71:40-9.
19. Kolpakov V, Rekhter MD, Gordon D, Wang WH, Kulik TJ. Effect of mechanical forces on growth and matrix protein synthesis in the in vitro pulmonary artery. Analysis of the role of individual cell types. Circ Res 1995;77:823-31.
20. Seliktar D, Nerem RM, Galis ZS. Mechanical strain-stimulated remodeling of tissue-engineered blood vessel constructs. Tissue Eng 2003;9:657-66.
21. Jones JA, McNally AK, Chang DT, Qin LA, Meyerson H, Colton E, et al. Matrix metalloproteinases and their inhibitors in the foreign body reaction on biomaterials. J Biomed Mater Res A 2008;84:158-66.
22. Hu J, Van den Steen PE, Sang QX, Opdenakker G. Matrix metalloproteinase inhibitors as therapy for inflammatory and vascular diseases. Nat Rev Drug Discov 2007;6:480-98.
23. Davis V, Persidskaia R, Baca-Regen L, Itoh Y, Nagase H, Persidsky Y, et al. Matrix metalloproteinase-2 production and its binding to the matrix are increased in abdominal aortic aneurysms. Arterioscler Thromb Vasc Biol 1998;18:1625-33.
24. Goumans MJ, Liu Z, ten Dijke P. TGF-beta signaling in vascular biology and dysfunction. Cell Res 2009;19:116-27.
25. Habashi JP, Judge DP, Holm TM, Cohn RD, Loeys BL, Cooper TK, et al. Losartan, an AT1 antagonist, prevents aortic aneurysm in a mouse model of Marfan syndrome. Science 2006;312:117-21.
26. Brooke BS, Habashi JP, Judge DP, Patel N, Loeys B, Dietz HC 3rd. Angiotensin II blockade and aortic-root dilation in Marfan's syndrome. N Engl J Med 2008;358:2787-95.

Submitted Jan 9, 2014; accepted Mar 7, 2014.

Journal of Neuroimmunology 269 (2014) 56–61

Contents lists available at ScienceDirect

Journal of Neuroimmunology

journal homepage: www.elsevier.com/locate/jneuroim

Increased number of Hassall's corpuscles in myasthenia gravis patients with thymic hyperplasia ☆

Naoko Matsui [a,b,*], Izumi Ohigashi [b], Keijirou Tanaka [a], Mie Sakata [b], Takahiro Furukawa [a], Yasushi Nakagawa [b,c], Kazuya Kondo [c], Tetsuya Kitagawa [d], Sumimasa Yamashita [e], Yoshiko Nomura [f], Yousuke Takahama [b], Ryuji Kaji [a]

[a] Department of Neurology, Institute of Health Bioscience, Graduate School of Medical Sciences, The University of Tokushima, Tokushima, Japan
[b] Division of Experimental Immunology, Institute for Genome Research, Graduate School of Medical Sciences, The University of Tokushima, Tokushima, Japan
[c] Department of Oncological Regenerative Surgery, Institute of Health Bioscience, Graduate School of Medical Sciences, The University of Tokushima, Tokushima, Japan
[d] Department of Cardiovascular Surgery, Institute of Health Bioscience, Graduate School of Medical Sciences, The University of Tokushima, Tokushima, Japan
[e] Division of Child Neurology, Kanagawa Children's Medical Center, Kanagawa, Japan
[f] Segawa Neurological Clinic for Children, Tokyo, Japan

ARTICLE INFO

Article history:
Received 29 July 2013
Received in revised form 14 January 2014
Accepted 22 January 2014

Keywords:
Myasthenia gravis
Thymus
Hassall's corpuscle
Medullary thymic epithelial cell
Thymic hyperplasia

ABSTRACT

The thymus is implicated as an organ that contributes to autoimmunity in myasthenia gravis (MG) patients. Hassall's corpuscles (HCs) are assumed to represent the terminally differentiated stage of medullary thymic epithelial cells (mTECs). By using multicolor immunohistofluorescence analysis, we examined HCs in thymuses that were therapeutically excised from MG (+) and MG (−) patients. We found that the number of HCs per unit area of the thymic medulla was significantly elevated in the thymuses of MG (+) patients with thymic hyperplasia. CCL21 expression increased in the hyperplastic MG thymuses. We speculate that the altered differentiation of mTECs is associated with the thymic hyperplasia and the onset of MG.

1. Introduction

Myasthenia gravis (MG) is a neurological autoimmune disease caused by autoantibodies against components of the neuromuscular junction. Muscle weakness can remain localized to one group of muscles, usually the eye muscles (ocular type), or spread to a large spectrum of skeletal muscles (generalized type). Antibodies against the acetylcholine receptor (AChR) are detectable in approximately 85% of patients with generalized MG (Vincent et al., 2001). The thymuses of MG patients often contain the components required to produce an immune response against AChR and are assumed to be one of the sources of AChR-specific antibodies (Vincent, 2002). In most seropositive patients with early-onset MG, the thymus is typically enlarged and contains many germinal centers (GCs) with B cell areas very similar to those seen in lymph nodes (Kirchner et al., 1986).

Importantly, the thymic medulla provides central self-tolerance in terms of the deletion of autoreactive T cells and the generation of regulatory T cells (Treg) (Nitta et al., 2008). However, our previous study indicated that the cellularity of Treg in the thymus and the circulation was not diminished in MG patients (Matsui et al., 2010). The promiscuous expression of a set of self-antigens is partly controlled by autoimmune regulator (AIRE) in medullary thymic epithelial cells (mTECs) (Anderson et al., 2002; Derbinski et al., 2005). A previous study demonstrated that AIRE controlled the expression of CHRNA1 messenger RNA, which encodes the α-subunit of human muscle AChR, in human mTECs, suggesting that mTECs set the threshold for self-tolerance versus autoimmunity in the context of MG (Giraud et al., 2007). Hassall's corpuscles (HCs), which are structures in the thymic medulla, were proposed to function in the removal of apoptotic thymocytes or the maturation of developing thymocytes (Blau, 1965; Senelar et al., 1976). There was also a report suggesting that human HCs activate dendritic cells, which in turn induce the generation of Treg (Watanabe et al., 2005). In addition, it was suggested that HCs represent the terminally differentiated stage of mTECs (Yano et al., 2008; White et al., 2010). However, the exact role of HCs remains vaguely understood. To better understand how self-tolerance in the immune system collapses in MG patients, we analyzed thymuses of MG patients with focus on HCs.

☆ Disclosure: The authors report no disclosures.

* Corresponding author at: Department of Neurology, Institute of Health Bioscience, Graduate School of Medical Sciences, The University of Tokushima, 3-18-15 Kuramoto, Tokushima 770-8503, Japan. Tel.: +81 88 633 7207; fax: +81 88 633 7208.
E-mail address: nao-mm@clin.med.tokushima-u.ac.jp (N. Matsui).

0165-5728/$ – see front matter © 2014 Elsevier B.V. All rights reserved.
http://dx.doi.org/10.1016/j.jneuroim.2014.01.011

2. Material and methods

2.1. Patients

The demographic data and clinical information of patients and control subjects are summarized in Table 1. The diagnosis of MG was made based on standard criteria (Vincent et al., 2001). Thymus specimens were obtained during cardiac surgery from MG (−) infants and adults having heart disease, or during thymectomy from MG (−) adults with thymoma and AChR-positive generalized MG (+) patients. The thymuses were classified as follows: MG (−) infants (n = 8), MG (−) adults without neoplasm (n = 8), MG (−) adults with thymoma (n = 8), MG (+) without hyperplasia or neoplasm (n = 9), MG (+) with hyperplasia (n = 7), and MG (+) with thymoma (n = 9). Pathological diagnosis was based on the analysis of hematoxylin–eosin (HE) stained sections. None of the MG (+) patients enrolled in this study took corticosteroids or immunosuppressants before the thymectomy. The procedures followed were in accordance with the Helsinki Declaration of 1975, as revised in 1983. This study was approved by the Ethics Committee of the Tokushima University Hospital. All subjects gave written informed patient consent for their participation.

2.2. Immunofluorescence analysis

Frozen thymus tissues embedded in OCT compound (Sakura) were sliced into 7 μm thick sections and fixed with acetone. The sections were incubated for 60 min at room temperature with a blocking reagent (ImmunoBlock) and stained with fluorescein isothiocyanate (FITC)-conjugated anti-CD4 antibody (clone MEM-241/OKT-4, Exbio), allophycocyanin (APC)-conjugated anti-CD8 antibody (clone OKT-8, eBioscience), and mouse anti-involucrin antibody (clone SY5, Abcam), followed by Alexa 546-conjugated anti-mouse immunoglobulin (Ig) antibody (Molecular Probes). Sections stained with biotinylated anti-involucrin (clone SY5) and anti-Ki-67 (clone MIB-1, Dako) antibodies were visualized with Alexa 488-conjugated streptavidin and Alexa 633-conjugated anti-mouse Ig antibody, respectively. Sections stained with anti-keratin 14 (clone AF64, Covance), biotinylated anti-involucrin (clone SY5), and anti-CCL21 (clone 54125, R&D Systems) antibodies were visualized with FITC-conjugated anti-rabbit Ig, Alexa 568-conjugated streptavidin, and Alexa 633-conjugated anti-mouse Ig antibodies, respectively. The hyperplastic samples were also stained with FITC-conjugated anti-CD19 antibody (clone HD37, Dako) and biotinylated anti-CD38 antibody (clone HIT2, Exbio), followed by Alexa 633-conjugated streptavidin (Molecular Probes). Immunofluorescence images were obtained with a Leica confocal microscope. Thymic sections containing parenchymal lobules were determined by HE staining. Up to six lobules per unit thymic section were examined to quantify the number of HCs per unit area of the thymic medulla as well as the areas of individual HCs, the area of medulla per unit lobule, and the area of cortex per unit lobule. In the specimens with thymoma, non-neoplastic tissues adjacent to the thymoma were analyzed. The corticomedullary architecture of the thymus was visualized by the predominant localization of CD4/CD8 double-positive thymocytes in the cortex and CD4/CD8 single-positive thymocytes in the medulla. Involucrin (+) concentric cellular clusters were identified as HCs. The number of HCs was defined by the number of HCs per unit area of the thymic medulla (mm^2). The area of HCs was calculated by tracing the periphery of involucrin (+) cell clusters. Quantification of the areas of HC (μm^2), medulla (mm^2), and cortex (mm^2) was performed by ImageJ software.

2.3. RT-PCR analysis

Total thymic RNA was extracted with Isogen (Wako Pure Chemical). cDNA was synthesized using oligo-dT primer and Superscript III reverse transcriptase (Invitrogen Life Technologies). Quantitative real-time PCR was performed using SYBR Premix Ex Taq (Takara Bio Inc.) and Light Cycler D × 400 (Roche). Amplified signals were confirmed to be single bands by gel electrophoresis and were normalized to the signals of the housekeeping gene, glyceraldehyde 3-phosphate dehydrogenase (GAPDH). Relative quantification and calculation of the range of confidence were performed by means of the comparative $2^{-\Delta\Delta C_T}$ method. mRNA expression normalized to GAPDH expression in the thymus of MG (−) adult was represented by 1.0 as the mean value. Primer sequences were as follows: CCL19, 5′-CATCGTGAGGAACTTCCACT-3′ and 5′-CTGCACGGTCATAGGTTAAC-3′; CCL21, 5′-CCTTGCCACACTCTTTCT CCC-3′ and 5′-CAAGGAAGAGGTGGGGTGTA-3′; AIRE, 5′-GAACGGGATT CAGACCATGT-3′ and 5′-TCTTCGAACTTGCTGGGAGT-3′; CHRNA1, 5′-TCGTCACCCACTTTCCCTTT-3′ and 5′-CCGCTCTCCATGAAGTTGCT-3′; and GAPDH, 5′-ACCCACTCCTCCACCTTTGA-3′ and 5′-TGGTGGTCCAGG GGTCTTAC-3′.

2.4. Statistical analysis

Data analyses were performed using Prism (GraphPad Software, San Diego, CA) and SPSS 20 (IBM, Chicago, IL) software. The Kruskal–Wallis test or the chi-square test was performed to assess differences in clinical data, immunofluorescence analysis, and RT-PCR analysis among the five

Table 1
Thymus samples and demographic/clinical information.

	Sex	Age, yr	Duration, yr	Ab titer	MGFA clinical classification, n (%)				
	Female (%)	Mean ± SD	Mean ± SD	Mean ± SD	I	II	III	IV	V
MG (−) (n = 24)									
Infants (n = 8)	5 F (63%)	1 ± 1[a, b]							
Adults (n = 16)	8 F (50%)	53 ± 16[a]							
No neoplasm (n = 8)	2 F (25%)	55 ± 17[b]							
Thymoma (n = 8)	6 F (75%)	50 ± 15							
MG (+) (n = 25)	20 F (80%)	45 ± 16	2.1 ± 3.8	258 ± 1093					
Normal (n = 9)	6 F (67%)	45 ± 12	2.7 ± 3.3[c]	37 ± 28	0 (0)	7 (78)	2 (22)	0 (0)	0 (0)
Hyperplasia (n = 7)	7 F (100%)	37 ± 17	3.9 ± 6.5[d]	847 ± 2053	0 (0)	4 (57)	3 (43)	0 (0)	0 (0)
Thymoma (n = 9)	7 F (78%)	52 ± 17	0.4 ± 0.4[c, d]	22 ± 18	0 (0)	5 (56)	3 (33)	1 (11)	0 (0)

Normal = no hyperplasia and no neoplasm.
Hyperplasia = thymic hyperplasia.
Age = age at thymectomy.
Duration = period between disease onset and thymectomy.
Ab = anti-acetylcholine receptor (AChR) antibody (normal < 0.2 nmol/L).
MGFA = Myasthenia Gravis Foundation of America.
[a] $p < 0.05$: compared to MG (−) infant group and MG (−) adult group.
[b] $p < 0.05$: compared to MG (−) infant group and MG (−) adult no neoplasm group.
[c] $p < 0.05$: compared to MG (+) normal group and MG (+) thymoma group.
[d] $p < 0.05$: compared to MG (+) hyperplasia group and MG (+) thymoma group.

groups. When significant results were obtained, multiple comparisons among subgroups were performed using Tukey's multiple comparison tests. Comparisons with $p < 0.05$ were considered to be significant.

3. Results

3.1. Number of HCs increased in thymuses of MG (+) patients with thymic hyperplasia

HCs that formed concentric ring structures in the thymic medulla were identified as involucrin (+) epithelial cell clusters (Fig. 1A). The number of HCs per unit area of the thymic medulla was large in infants but decreased in adults (Fig. 1B). However, the number of HCs was elevated in the thymuses of MG (+) patients with thymic hyperplasia, compared with those in the other adult groups (Fig. 1C). HCs were predominantly detected around GCs in the thymuses of those patients (Fig. 1B). The thymuses in the other MG subgroups did not show an increase in the number of HCs (Fig. 1B, C). The areas of HCs in all the groups examined were not significantly different (Fig. 1D). The medullary area, but not the cortical area, of the thymuses of MG (+) patients with thymic hyperplasia, was significantly larger than that of MG (+) patients without the thymic hyperplasia (Fig. 1E, F).

3.2. Morphology of HCs

HE staining enabled visualization of reddish concentric structures in accordance with previously described HCs. Analysis of the HE-stained sections supported the findings described above (data not shown). A fraction of large HCs exhibited calcification in all of the patient groups examined (Fig. 2A, arrows). The calcification was found in the thymus irrespective of the presence or absence of MG (Fig. 2A). However, we also noted that the calcification in HCs detected in the thymic specimens from MG (+) patients with thymic hyperplasia tended to localize at the periphery of HCs (Fig. 2A), suggesting that HCs in MG (+) patients with thymic hyperplasia are morphologically different from HCs in the other groups. Very few HCs in all the groups, including the MG (+) group with thymic hyperplasia, were stained for Ki-67, a marker of active cellular proliferation and ribosomal RNA transcription (Fig. 2B), suggesting that the cells in HCs from all the groups examined in this study are not actively proliferating.

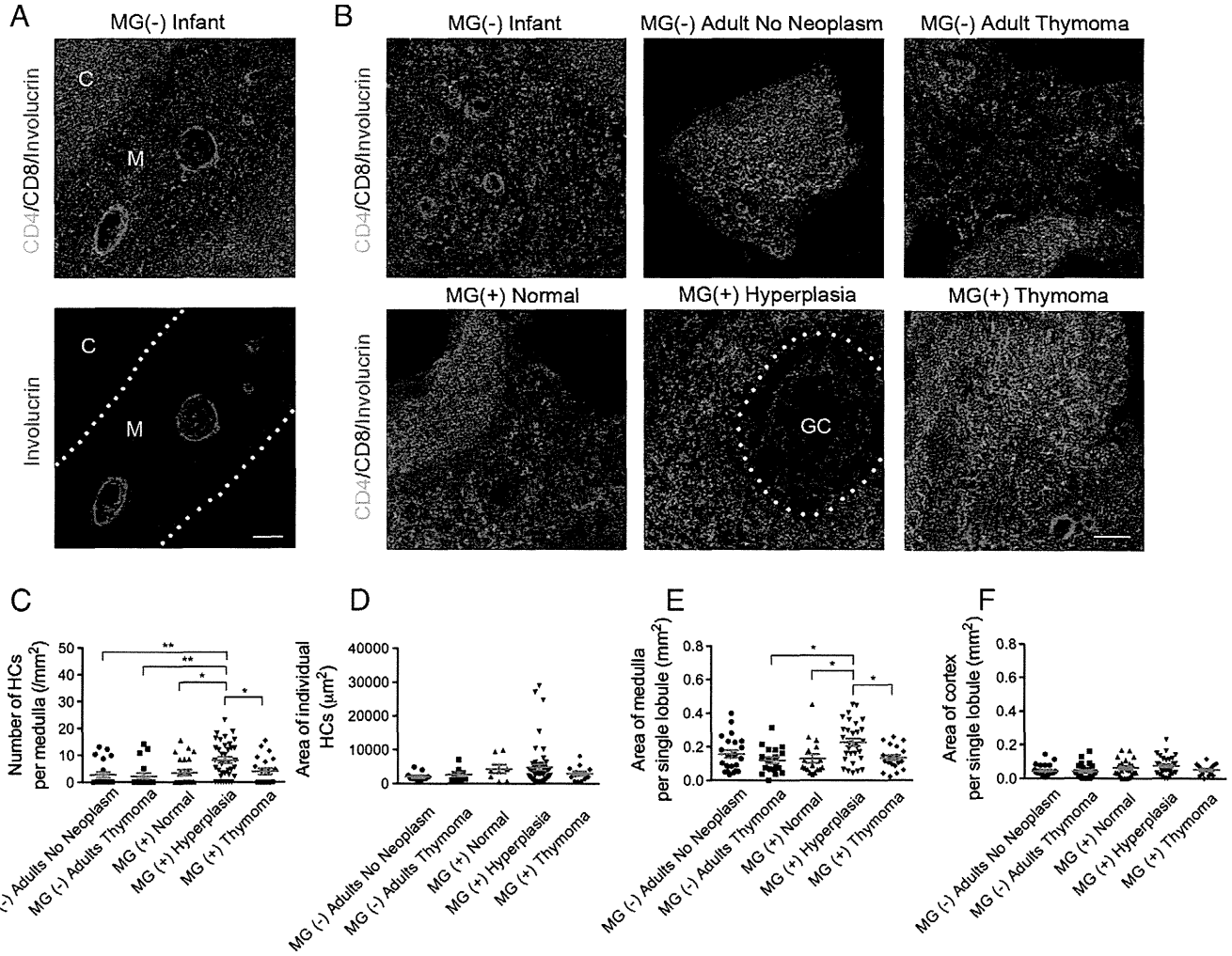

Fig. 1. Immunofluorescence analysis of Hassall's corpuscles in human thymus. (A) Thymic sections from a 3-month-old infant were stained for CD4 (green), CD8 (blue), and involucrin (red). Cells in cyan indicate the co-expression of CD4 and CD8, and are therefore $CD4^+CD8^+$. Bottom image shows the distribution of involucrin signals (red) in the area identical to the top image. Dotted lines indicate cortico-medullary junctions. C, cortex; M, medulla. Scale bar: 100 μm. (B) Representative results of immunofluorescence analysis. Top three figures show MG (−) thymus and bottom three figures show MG (+) thymus. GC, germinal center. Scale bar: 100 μm. (C–F) Quantitative analysis of immunohistochemically stained sections. Number of HCs per unit area of thymic medulla (/mm²) (C), areas of individual HCs (μm²) (D), area of medulla per unit lobule (mm²) (E), and area of cortex per unit lobule (mm²) (F) in the thymuses of indicated individuals. Horizontal red lines represent means and standard errors of the data. *$p < 0.05$; **$p < 0.01$

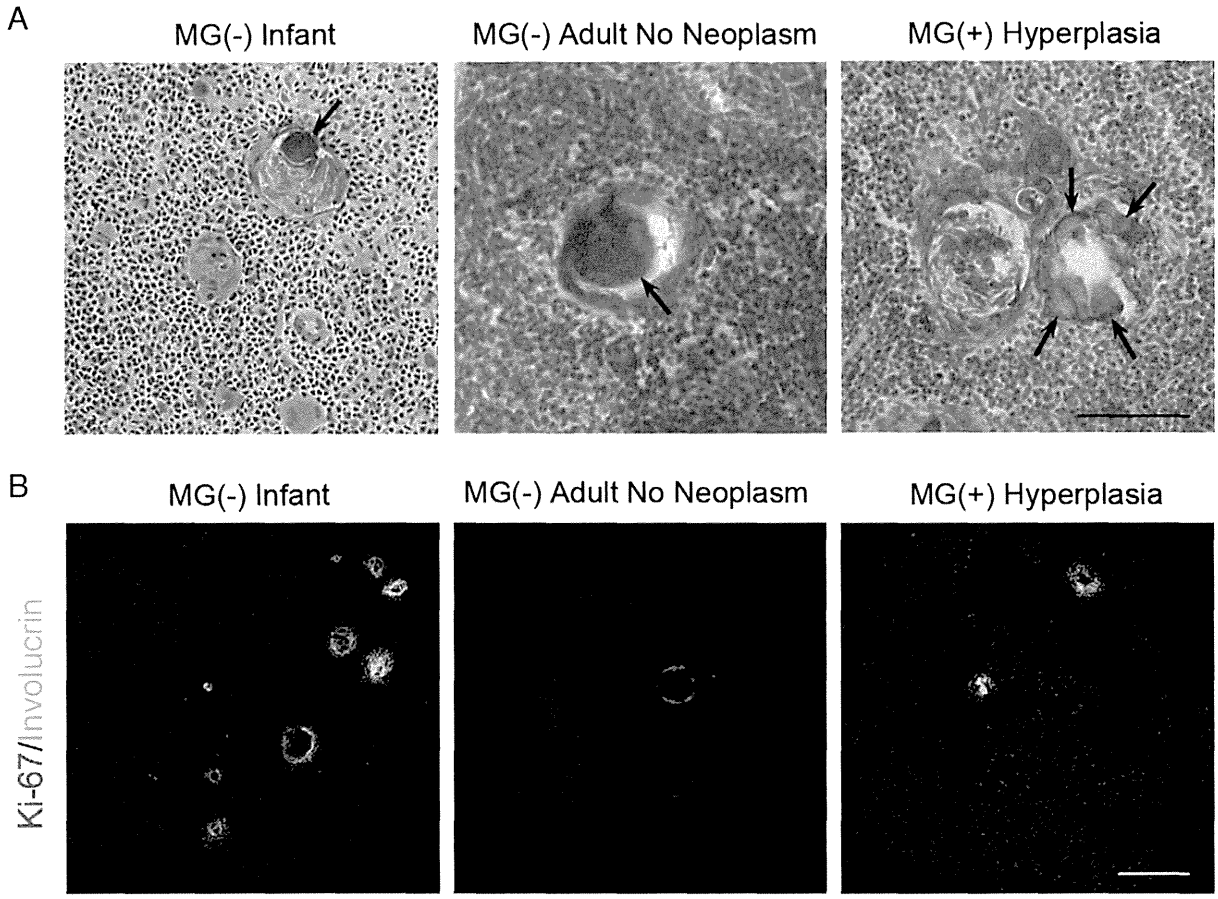

Fig. 2. Morphology of Hassall's corpuscles in thymuses of MG patients. (A) Representative images of HE-stained HCs. Calcification is detected as the light purple structure in HCs (arrows). Scale bar: 100 μm. Representative immunofluorescence images for Ki-67 (red) and involucrin (green). Scale bar: 200 μm.

3.3. CCL21 expression increased in MG (+) patients with thymic hyperplasia

We examined the expression of the following mRNAs, which are associated with mTEC function in self-tolerance. CC-chemokine ligand 19 (CCL19) and CCL21 are produced by mTECs and are critical for the establishment of self-tolerance in T cells (Ueno et al., 2004; Kurobe et al., 2006). CHRNA1 expression by mTECs is regulated by AIRE and implicated in the self-tolerance to AChR (Giraud et al., 2007). We found a significant increase in CCL21 mRNA expression in the thymuses of MG (+) patients with thymic hyperplasia compared to the other groups, including the non-MG adults. However, there was no significant difference in CCL19 or CHRNA1 mRNA expression in the thymuses of patients of all the groups, including the MG (+) patients with thymic hyperplasia (Fig. 3). We could not detect the expression of AIRE in this study (data not shown). CCL21 immunoreactivities in the thymus, which were predominantly detected in the medullary region containing involucrin positive HCs, were much more prominent in the thymuses of MG (+) patients with thymic hyperplasia than in the other groups (Fig. 4).

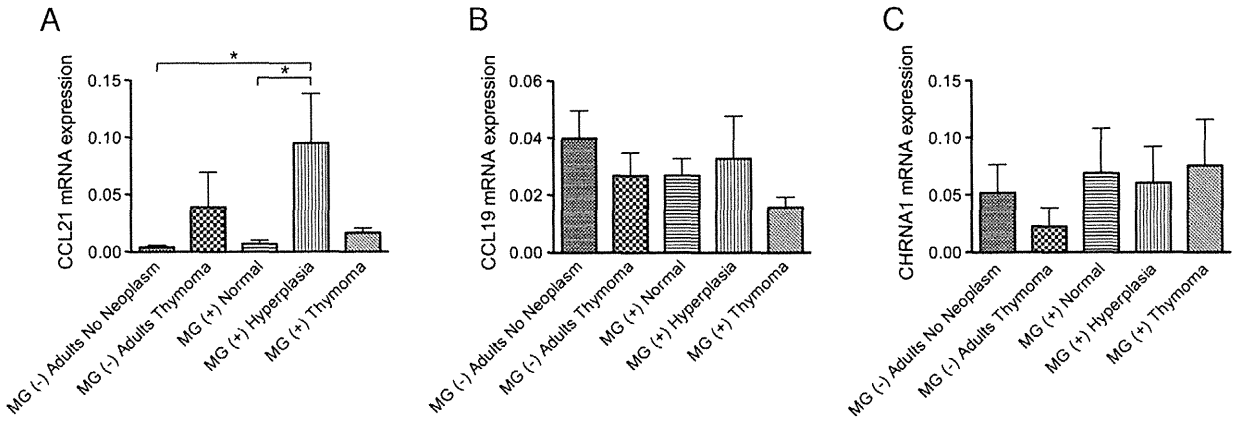

Fig. 3. Quantitative polymerase chain reaction analysis of CCL21, CCL19, and CHRNA1 mRNA expression in MG (−) and MG (+) thymuses. *$p < 0.05$.

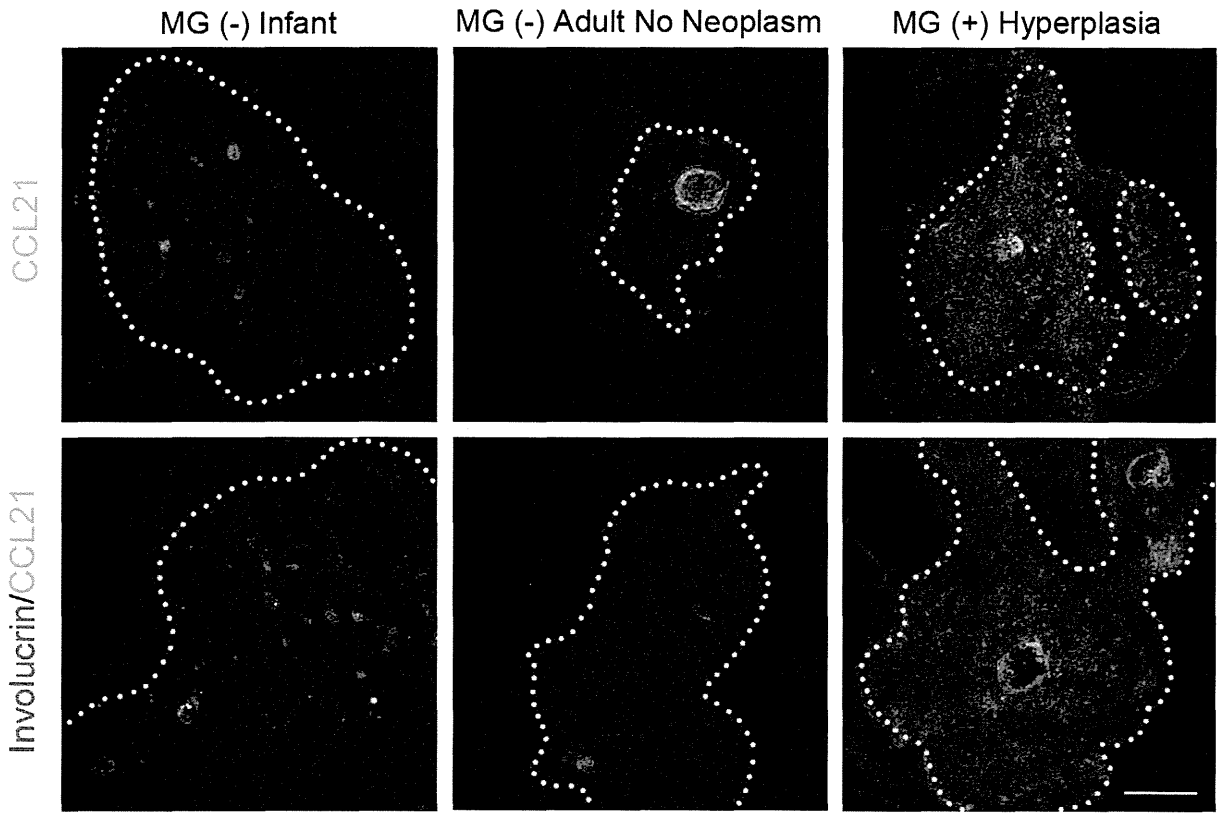

Fig. 4. Immunofluorescence analysis of CCL21 expression in human thymus. Representative images of involucrin signals (red) and CCL21 ones (green) in the thymus. Dotted lines indicate the cortico-medullary junctions as determined by co-staining with anti-K14 specific antibody, which detects the medullary region. Scale bar: 200 μm.

4. Discussion

In this study, we showed that the number of HCs per unit area of the thymic medulla increased in the thymuses of MG (+) patients with thymic hyperplasia. The thymic medulla is a specialized microenvironment where developing thymocytes establish central self-tolerance through the deletion of pathogenic T cells (for instance, T cells specific for AChR) and the generation of Treg. HCs, which express involucrin, are assumed to represent the terminally differentiated stage of mTECs (White et al., 2010). The increase in the number of HCs in the thymuses of MG (+) patients with thymic hyperplasia suggested that the terminal differentiation of mTECs is altered in those patients. Indeed, we found that HCs in MG (+) patients with thymic hyperplasia were morphologically different from HCs in the other patient groups. We also noted the increase in CCL21 mRNA expression in the thymuses of MG (+) patients with thymic hyperplasia. Accordingly, CCL21 protein expression in the thymic medulla was elevated in the thymuses of MG (+) patients with thymic hyperplasia. Since it was previously described that CCL21 expressed by mTECs participated in the medullary migration of positively selected thymocytes, which was essential for the establishment of self-tolerance (Ueno et al., 2004; Kurobe et al., 2006), it is possible that the increased CCL21 expression by the developmentally altered mTECs in the hyperplastic MG thymus contributes to the recruitment of pathogenic lymphocytes, resulting in the development of immune response to AChR. It is also possible that CCL21 overexpression causes the infiltration of naïve B cells into the hyperplastic MG thymus, as previously suggested (Le Panse et al., 2006; Berrih-Aknin et al., 2009).

The exact role of HCs remains unclear. A previous study demonstrated that HCs in the thymuses of X-irradiated animals increased in size and number (Blau and Veall, 1967). Another study showed that sublethal irradiation caused modifications in the thymic microenvironment, including the alteration of mTECs (Randle-Barrett and Boyd, 1995). Those findings suggest that an altered thymic microenvironment induced by irradiation-mediated stress leads to an increase in the number of HCs in the thymus. It was previously reported that hyperplastic thymuses associated with MG showed an elevation of insulin-like growth factor I (IGF-I) expression in thymic epithelial cells, including HCs, and large HCs were detected in those thymuses (Marinova et al., 2008). Altogether, it is conceivable that the altered development of mTECs, including the increase in the number of HCs and the elevation of CCL21 expression, is associated with thymic hyperplasia and the onset of MG.

Acknowledgments

This research was partially supported by Japan Society for the Promotion of Science Grants-in-Aid for Young Scientists (B), 23790995, 2012 and 25870477, 2013. This work was also supported by grants from the Neuroimmunological Disease Research Committee and the Ministry of Health, Labour and Welfare, Japan.

References

Anderson, M.S., Venanzi, E.S., Klein, L., Chen, Z., Berzins, S.P., Turley, S.J., von Boehmer, H., Bronson, R., Dierich, A., Benoist, C., Mathis, D., 2002. Projection of an immunological self shadow within the thymus by AIRE protein. Science 298, 1395–1401.

Berrih-Aknin, S., Ruhlmann, N., Bismuth, J., Cizeron-Clairac, G., Zelman, E., Shachar, I., Dartevelle, P., de Rosbo, N.K., Le Panse, R., 2009. CCL21 overexpressed on lymphatic vessels drives thymic hyperplasia in myasthenia. Ann. Neurol. 66, 521–531.

Blau, J.N., 1965. A phagocytic function of Hassall's corpuscles. Nature 208, 564–567.

Blau, J.N., Veall, N., 1967. The uptake and localization of proteins, Evans Blue and carbon black in the normal and pathological thymus of the guinea-pig. Immunology 12, 363–372.

Derbinski, J., Gäbler, J., Brors, B., Tierling, S., Jonnakuty, S., Hergenhahn, M., Peltonen, L., Walter, J., Kyewski, B., 2005. Promiscuous gene expression in thymic epithelial cells is regulated at multiple levels. J. Exp. Med. 202, 33–45.

Giraud, M., Taubert, R., Vandiedonck, C., Ke, X., Lévi-Strauss, M., Pagani, F., Baralle, F.E., Eymard, B., Tranchant, C., Gajdos, P., Vincent, A., Willcox, N., Beeson, D., Kyewski, B., Garchon, H.J., 2007. An IRF8-binding promoter variant and AIRE control CHRNA1 promiscuous expression in thymus. Nature 448, 934–937.

Kirchner, T., Schalke, B., Melms, A., von Kügelgen, T., Müller-Hermelink, H.K., 1986. Immunohistological patterns of non-neoplastic changes in the thymus in myasthenia gravis. Virchows Arch. B. Cell Pathol. Incl. Mol. Pathol. 52, 237–257.

Kurobe, H., Liu, C., Ueno, T., Saito, F., Ohigashi, I., Seach, N., Arakaki, R., Hayashi, Y., Kitagawa, T., Lipp, M., Boyd, R.L., Takahama, Y., 2006. CCR7-dependent cortex-to-medulla migration of positively selected thymocytes is essential for establishing central tolerance. Immunity 24, 165–177.

Le Panse, R., Cizeron-Clairac, G., Bismuth, J., Berrih-Aknin, S., 2006. Microarrays reveal distinct gene signatures in the thymus of seropositive and seronegative myasthenia gravis patients and the role of CC chemokine ligand 21 in thymic hyperplasia. J. Immunol. 177, 7868–7879.

Marinova, T.T., Kuerten, S., Petrov, D.B., Angelov, D.N., 2008. Thymic epithelial cells of human patients affected by myasthenia gravis overexpress IGF-I immunoreactivity. APMIS 116, 50–58.

Matsui, N., Nakane, S., Saito, F., Ohigashi, I., Nakagawa, Y., Kurobe, H., Takizawa, H., Mitsui, T., Kondo, K., Kitagawa, T., Takahama, Y., Kaji, R., 2010. Undiminished regulatory T cells in the thymus of patients with myasthenia gravis. Neurology 74, 816–820.

Nitta, T., Murata, S., Ueno, T., Tanaka, K., Takahama, Y., 2008. Thymic microenvironments for T-cell repertoire formation. Adv. Immunol. 99, 59–94.

Randle-Barrett, E.S., Boyd, R.L., 1995. Thymic microenvironment and lymphoid responses to sublethal irradiation. Dev. Immunol. 4, 101–116.

Senelar, R., Escola, M.J., Escola, R., Serrou, B., Serre, A., 1976. Relationship between Hassall's corpuscles and thymocytes fate in guinea-pig foetus. Biomedicine 24, 112–122.

Ueno, T., Saito, F., Gray, D.H., Kuse, S., Hieshima, K., Nakano, H., Kakiuchi, T., Lipp, M., Boyd, R.L., Takahama, Y., 2004. CCR7 signals are essential for cortex-medulla migration of developing thymocytes. J. Exp. Med. 200, 493–505.

Vincent, A., 2002. Unravelling the pathogenesis of myasthenia gravis. Nat. Rev. Immunol. 2, 797–804.

Vincent, A., Palace, J., Hilton-Jones, D., 2001. Myasthenia gravis. Lancet 357, 2122–2128.

Watanabe, N., Wang, Y.H., Lee, H.K., Ito, T., Wang, Y.H., Cao, W., Liu, Y.J., 2005. Hassall's corpuscles instruct dendritic cells to induce CD4+CD25+ regulatory T cells in human thymus. Nature 436, 1181–1185.

White, A.J., Nakamura, K., Jenkinson, W.E., Saini, M., Sinclair, C., Seddon, B., Narendran, P., Pfeffer, K., Nitta, T., Takahama, Y., Caamano, J.H., Lane, P.J., Jenkinson, E.J., Anderson, G., 2010. Lymphotoxin signals from positively selected thymocytes regulate the terminal differentiation of medullary thymic epithelial cells. J. Immunol. 185, 4769–4776.

Yano, M., Kuroda, N., Han, H., Meguro-Horike, M., Nishikawa, Y., Kiyonari, H., Maemura, K., Yanagawa, Y., Obata, K., Takahashi, S., Ikawa, T., Satoh, R., Kawamoto, H., Mouri, Y., Matsumoto, M., 2008. AIRE controls the differentiation program of thymic epithelial cells in the medulla for the establishment of self-tolerance. J. Exp. Med. 205, 2827–2838.